

# Constitutive relations and linear stability of a sheared granular flow

By V. KUMARAN

Department of Chemical Engineering, Indian Institute of Science, Bangalore 560 012, India

(Received 31 January 2003 and in revised form 9 September 2003)

The constitutive relation for the granular flow of smooth, nearly elastic particles ( $(1 - e) \ll 1$ ) is derived in the adiabatic limit, where the length scale for conduction,  $\lambda/(1 - e)^{1/2}$ , is small compared to the macroscopic scale. Here,  $\lambda$  is the mean free path and  $e$  is the coefficient of restitution. In this case, energy is convected by the mean flow, and the rate of change of the energy in a Lagrangian reference frame is determined by a balance between the rate of production (due to the shear) and the rate of dissipation (due to inelastic collisions). A Gaussian approximation is used for the velocity distribution function, and the velocity variance is determined from a balance equation for the second moment of the velocity distribution using an asymptotic expansion in the small parameter  $\epsilon = (1 - e)^{1/2}$ . The stress tensor is then determined from the velocity variance. It is found that the leading-order,  $O(\epsilon)$  and  $O(\epsilon^2)$  contributions to the stress tensor are identical in form to those in the Euler, Navier–Stokes and Burnett approximations, and the numerical values of these coefficients are close to those calculated using the Enskog procedure. The stress tensor is used to obtain analytical expressions for the growth rates of the hydrodynamic modes in a linear shear flow in the limit where the wavelength is long compared to the length scale of conduction. In the plane of flow, transverse momentum perturbations are found to be stable, while perturbations in the density and longitudinal momenta grow exponentially at short times and decay in the long-time limit. It is found that the Navier–Stokes approximation captures the leading behaviour of the growth rate in the small-wavenumber limit for perturbations in the plane of flow. In the vorticity direction, it is found that the Navier–Stokes approximation is not adequate to capture the leading behaviour in the small-wavenumber limit, and dominant terms in the growth rates of the transverse modes depend on the Burnett coefficients. Perturbations in this direction are unstable at low density, but become stable as the density is increased. When the wave length is small compared to the conduction length, the rate of conduction of energy is large compared to the rate of dissipation, and the hydrodynamic modes are identical to those for a gas of elastic particles at equilibrium. The hydrodynamic modes are all stable in this case. The transition between these two regimes is examined for a dilute granular flow, and a transition from unstable to stable modes is predicted as the wavenumber is increased. The analysis indicates that the minimal model which accurately captures the dynamics in both limits is one in which the constitutive relation for the stress incorporates the strain-rate-dependent Burnett terms in the stress equation (neglecting the temperature-dependent Burnett terms), and the constitutive relation for the heat flux is the Fourier law for heat conduction (neglecting all the Burnett terms).

---

## 1. Introduction

A granular material consisting of particles of diameter  $d$  and coefficient of restitution  $e$  is subjected to a shear flow with deformation rate  $G_{ij}$ . For a linear shear flow where there is only one non-zero component of the rate of deformation tensor  $G_{xy}$ , the form of the shear stress can be deduced from dimensional analysis,

$$\sigma_{xy} = A(\phi, e)md^{-1}G_{xy}^2, \quad (1)$$

where  $A(\phi, e)$  is a dimensionless constant,  $\phi$  is the volume fraction of the particles, and  $m$  is the particle mass. The above relation, called the Bagnold law, has been used previously for simple shear flows. However, dimensional analysis does not indicate how this could be extended for a more general case, where the rate of deformation tensor and the stress tensor have many non-zero components. For the case of a dilute granular flow, when the coefficient of restitution is close to 1, kinetic theory techniques can be used to determine the correct form of the constitutive relation. In the kinetic theory of gases (Chapman & Cowling 1970; Resibois & de Leener 1977), the Navier–Stokes equations for the conserved (‘slow’) variables are derived by taking moments of the Boltzmann equation. In a fluid of elastic particles, mass, momentum and energy constitute the conserved variables, because these are conserved in particle collisions, while the fluctuations in the higher moments decay over time scales comparable to the time between collisions. In a gas of inelastic particles, it is expected that the energy is also a non-conserved (‘fast’) variable, since it is not conserved in a collision. Consequently, a hydrodynamic description should be derivable from equations for the conservation of mass and momentum. The ‘temperature’ would act as an active scalar which determines the viscometric coefficients, and which is determined, in a Lagrangian reference frame, by a balance between the rate of production due to the deformation and the rate of dissipation due to inelastic collisions.

Constitutive models have been developed for granular flows using methods similar to those used in the kinetic theory of gases (Savage & Jeffrey 1981; Jenkins & Savage 1983; Lun *et al.* 1984; Jenkins & Richman 1985). These models typically fall into two categories, the generalized Navier–Stokes equations where the mass and momentum equations are similar to those for a simple fluid, but where the energy equation has an additional term due to the dissipation of energy in inelastic collisions; and the moment expansion models (Jenkins & Richman 1985) where the higher moments of the velocity distribution function are incorporated in the description. There have been systematic derivations of kinetic equations up to Burnett order starting from the Boltzmann equation using an expansion with the Knudsen number and the inelasticity of the particle collisions as the small parameters (Sela, Goldhirsch & Noskovicz 1996; Sela & Goldhirsch 1998). All of these descriptions of granular flows do include the temperature (mean square velocity) as a dynamical variable for the following reason. If  $e$  is the coefficient of restitution, the energy dissipated in a collision between two particles is  $O((1-e)T)$ , where the granular temperature  $T$  is the mean square velocity of the particles (the particle mass is assumed to be 1 without loss of generality). It can be inferred, by examining the energy balance equation, that fluctuations in energy are damped over a length scale comparable to  $\lambda/(1-e)^{1/2}$ , where  $\lambda$  is the mean free path. The rate of diffusion of energy in the energy balance equation scales as  $O(D_T T/L^2)$ , where the thermal diffusivity  $D_T \sim \lambda T^{1/2}$  in the kinetic theory of gases, while the rate of dissipation of energy is  $O((1-e)T^{3/2}/\lambda)$ , since  $(T^{1/2}/\lambda)$  is the frequency of collisions. Equating these two terms, it is clear that the rate of diffusion and rate of dissipation are of equal magnitude for  $L \sim \lambda/(1-e)^{1/2}$ . The equation for the energy

flux also contains a term proportional to the density gradient which, from Sela & Goldhirsch (1998), is proportional to (in the present notation)  $\lambda T^{3/2}(1-e)\nabla\rho$ . The divergence of this flux, which enters into the energy balance equation, is proportional to  $(\lambda T^{3/2}(1-e)\rho/L^2)$ , while the rate of dissipation of energy per unit volume is proportional to  $((1-e)\rho T^{3/2}/\lambda)$ . The ratio of the divergence of the flux due to density variations and the rate of dissipation of energy is  $(\lambda^2/L^2)$ , and the contribution to the energy balance equation from the flux due to density gradients is important only for  $L \sim \lambda$ . The present analysis is restricted to  $L \gg \lambda$ , so this conduction term is not important in the present case.

In the limit  $(1-e) \ll 1$ , it is expected that energy fluctuations decay over distances large compared to the mean free path. In the limit  $L \ll \lambda/(1-e)^{1/2}$ , it is appropriate to treat energy as a conserved variable and write a transport equation for the energy. For  $L \gg \lambda/(1-e)^{1/2}$ , a hydrodynamic equation would not include the temperature as a dynamical variable, but only as an active scalar which is convected with the flow, and whose magnitude is determined by a balance between the source and dissipation of energy in a Lagrangian reference frame. However, in contrast to passive scalars which are merely advected by the flow, the temperature influences dynamical properties such as the coefficients of viscosity. There are several advantages to a formulation of this type. First, since the temperature equation does not contain spatial gradients (except for those which appear in the substantial derivative), it is not necessary to specify boundary conditions for the temperature and heat flux. The temperature boundary condition is found to be sensitive to the boundary configuration (Jenkins & Richman 1986), and a formulation which does not require temperature boundary conditions would not be sensitive to the specifics of the boundary configuration. The boundary configuration does influence the flow within a distance of the order of a conduction length  $\lambda/(1-e)^{1/2}$  from the boundary, but this can be neglected when the conduction length is small compared to the system size. Another advantage is that it is not necessary to include terms proportional to the gradients of the temperature in the stress equation. It should be noted, however, that this formulation applies only to flows where there is a source of energy due to the rate of deformation within the flow, such as a simple shear flow. It would not be applicable to flows where energy is produced at boundaries such as vibrated granular materials, since the conduction of energy is necessary to sustain the flow.

In the kinetic theory of gases (Chapman & Cowling 1970), the stress tensor at Burnett order contains terms which are proportional to the second spatial gradient of the temperature, and the square of the first gradient of the temperature. Similarly, the heat flux contains terms proportional to the rate of deformation. When conduction is neglected, these terms are no longer present in the stress equation, and so the equation for the stress becomes considerably simplified at Burnett and higher orders. The objective of the present analysis is to determine whether it is possible to obtain simplified constitutive relations when the conduction length is small compared to the macroscopic scale, and compare these with results from the kinetic theory for granular flows where the temperature is included as a dynamical variable, in order to examine whether this formulation accurately describes the dynamics of the flow.

In the present analysis, a constitutive relation for the stress tensor is obtained for the case  $(1-e) \ll 1$ , and  $L \gg \lambda/(1-e)^{1/2}$ , where the macroscopic scale is large compared to the conduction length. In this case, an asymptotic expansion in the parameter  $\epsilon = (1-e)^{1/2}$  can still be used to calculate the collision integral, but the energy equation simplifies to a local balance between the source of energy due to the deformation of the material and the dissipation due to inelastic collisions (adiabatic approximation).

The starting point for the analysis is the Boltzmann equation for the distribution function. The zeroth and first velocity moments of the Boltzmann equation provide the mass and momentum equations. Since mass and momentum are conserved in a collision, the decay rates of these modes approach zero in the long-wave limit. A Gaussian approximation is used for the higher moments, where the distribution function is assumed to be a Gaussian distribution, in which the temperature  $T_{ij}$ , which is the second moment of the velocity distribution, is a symmetric tensor. The Gaussian approximation has been used earlier by Jenkins & Richman (1988) for the second moments of the shear flow of inelastic disks, and the components of the stress were determined in the dense and dilute limits. A different formalism was adopted by Jenkins & Richman (1985), where Grad's 13-moment method was used to determine the moments of the velocity distribution. In the present analysis, an expansion in the parameter  $\epsilon$  is used to obtain a relation between  $T_{ij}$  and the rate-of-deformation tensor  $G_{ij}$ . This is inserted into the equation for the stress to obtain the constitutive relation as a series in the parameter  $\epsilon$ . This formalism is advantageous because it enables a direct comparison between the contribution to the stress tensor at different orders in  $\epsilon$ , and the contributions obtained in the Chapman–Enskog method which employs an expansion in the ratio of the mean free path and the macroscopic scale.

The mass and momentum equations reduce to the Navier–Stokes equations when the stress tensor correct to  $O(\epsilon)$  is used, and so this approximation is referred to as the Navier–Stokes approximation. The expression for the stress tensor correct to  $O(\epsilon^2)$ , referred to as the Burnett approximation, incorporates normal stress differences. The seven viscometric coefficients are explicitly calculated as a function of the volume fraction. It is found that the coefficients in the Burnett approximation evaluated here are numerically close to those obtained using the Enskog procedure in the kinetic theory of dilute gases, and are identical to those obtained using a simplified Enskog procedure when only the first term in the Sonine polynomial expansion for the distribution function is retained (Chapman & Cowling 1970). Thus, the results for the second-order closure scheme, when energy is treated as a non-conserved variable, are in agreement with the results of the Enskog procedure when energy is treated as a conserved variable. This agreement indicates that the anisotropic Gaussian approximation for the distribution function is close to the actual distribution function. The form of the stress tensor correct to  $O(\epsilon^3)$ , referred to as the super-Burnett approximation, is also deduced using symmetry arguments, but the viscometric coefficients are not explicitly calculated.

Though the terms Navier–Stokes, Burnett and super-Burnett are used here to denote different levels of approximation, it should be noted that the procedure used here is qualitatively different from that used for deriving macroscopic equations in the kinetic theory of gases. In that case, the mean free path  $\lambda$  is small compared to the length scale of the flow  $L$ , and the mean velocity  $U$  is small compared to the root mean square velocity of the gas  $T^{1/2}$ , so that an expansion is used in the gradients of the density, velocity and temperature. The number of spatial derivatives in the Burnett terms in the stress tensor is one higher than that in the Newton's law of viscosity. In gases at equilibrium, the Burnett equations have spurious high-wavenumber instabilities, owing to the presence of second spatial derivatives of the temperature and velocity fields in the expressions for stress. It is necessary to use viscoelastic relaxation models in order to avoid numerical difficulties associated with these instabilities (Jin & Slemrod 2001). However, these difficulties do not occur in the present formulation, because the expansion is carried out about the driven state, with

a non-zero strain rate, instead of an equilibrium state. Therefore, the Burnett terms contain the same number of spatial derivatives as the Navier–Stokes terms, though they are higher order in the parameter  $\epsilon$ . For example, if perturbations  $(u'_x, u'_y)$  are imposed about a base state with rate of deformation  $G_{xy}$ , the variation in the stress due to the Burnett term proportional to  $G_{xy}^2$  will have the form  $2G_{xy}(\partial_y u'_x + \partial_x u'_y)$ . This term contains one spatial derivative because the expansion is carried out about a driven state, in contrast to an equilibrium system where the same term will contain two spatial derivatives. Thus, the Burnett term in a driven system contains the same power of the wavenumber as the Navier–Stokes term, and it is the effect of lowest-order wavenumber terms that are analysed here. Consequently, instabilities due higher-order wavenumber terms are not encountered.

In the kinetic theory of gases, the Burnett coefficients can be calculated only in the dilute limit, where the assumption of molecular chaos is valid. When the number density increases, there is a contribution to the stress due to correlations in the particle positions prior to collision (Ernst *et al.* 1978). This contribution results in a non-analytic dependence of the stress on the rate of deformation. For a simple shear flow, in which the flow is in the  $x$ -direction and the gradient in the  $y$ -direction, the off-diagonal component of the stress is of the form  $\sigma_{xy} = \eta G_{xy} + \eta' G_{xy} |G_{xy}|^{1/2}$ , where  $G_{xy} = (\partial u_x / \partial y)$  is the rate of deformation. Consequently, the leading correction to Newton's law for the stress is proportional to  $|G_{xy}|^{3/2}$ , whereas the Burnett expansion assumes that the leading correction to Newton's law is a quadratic function of the rate of deformation. Consequently, Burnett coefficients evaluated in the usual way turn out to be infinite for systems at moderate density. However, as explained in detail by Ernst *et al.* (1978), there are several restrictions on the range of  $G_{xy}$  for which the calculation is valid. The most relevant restriction for the present analysis (4(iii) in the conclusions section of Ernst *et al.* 1978), is that  $(G_{xy}/T^{1/2} < k)$ , where  $k$  is the smallest wavenumber (inverse of the system size), and the applicability of this restriction is examined in further detail. For a granular flow, the temperature and the rate of deformation are related, since the rate of deformation is the source of energy which sustains the fluctuating velocity of the particles. An asymptotic analysis in the parameter  $\epsilon = (1 - e)^{1/2}$  is used in the present analysis, and the ratio  $(G_{xy}/T^{1/2}) \propto \epsilon \lambda^{-1}$ , where  $\lambda$  is the mean free path, and the contribution to the stress tensor proportional to  $\eta'$  is significant for  $(k\lambda) > \epsilon^{1/2}$ . However, the calculation of the Burnett coefficients is restricted to the low-wavenumber regime  $(k\lambda) \ll \epsilon$ , or  $(G_{xy}/T^{1/2}) \gg k$ . In this case, even though the second correction to the stress tensor is formally proportional to  $|G_{xy}|^{3/2}$  in a small  $G_{xy}$  expansion, it turns out that the rate of deformation is sufficiently large that the Burnett term proportional to  $G_{xy}^2$  is larger than the term proportional to  $|G_{xy}|^{3/2}$ . Consequently, the regular Burnett expansion is valid in this limit.

The growth rates of the hydrodynamic modes for a linear shear flow are determined in the long-wave limit in the second part of the analysis. The linear stability of a sheared granular flow has been the subject of many studies. Since the mean velocity is a linear function of the coordinate in the gradient direction, the equations for the perturbations to the density, velocity and temperature are functions of the spatial coordinate in an unbounded system, and a homogeneous eigenvalue problem cannot be formulated if the wave numbers are independent of time. In order to obtain spatially homogeneous equations, it is necessary to employ a time-dependent wave vector, whose component in the direction of flow is a function of time, so that the wave vector 'turns' with the mean flow. In this case, the equations for the perturbations are independent of the spatial coordinates, but dependent on time, and so the growth

or decay of perturbations is not exponential. Savage (1992) and Babic (1993) used a linear stability analysis to determine the rate of growth of perturbations in the limit of small time, when the growth is exponential. They found that perturbations are unstable in all three coordinate directions, and numerically identified the unstable domains in wavenumber space. Schmid & Kytomaa (1994) studied the stability of perturbations in the limit of long time, and showed that perturbations become stable in this limit. This indicates that there is a transient growth of perturbations with wavenumber in the flow direction, followed by stabilization at long times. However, the wave vectors in the gradient and vorticity directions are not functions of time, and the studies of Savage (1992) and Babic (1993) indicate that perturbations are unstable in these directions. There have been many subsequent studies of the linear stability of bounded and unbounded granular flows such as those of Wang, Jackson & Sundaresan (1996), and the conclusions of these studies have been qualitatively the same. All of these studies have used equations similar to the Navier–Stokes mass, momentum and energy equations to study the stability, with an additional energy dissipation term due to inelastic collisions in the energy equation.

Kumaran (2001*a, b*) used a moment expansion method to determine the stability of a granular flow in the dilute limit. In these studies, the dynamical variables were not restricted to the mass, momentum and energy, but higher moments of the velocity distribution function were also included. The growth rates of the hydrodynamic modes were determined in the limit of short time and small wavenumber, and it was found that the scaling of the growth rate with wavenumber was very different from that for elastic systems. In an elastic fluid (Resibois & de Leener 1977; Kamgar-Parsi & Cohen 1986), the growth rates of the five conserved modes, which are the mass, momenta and energy, decay to zero in the long-wave limit since these are conserved in binary collisions. The growth rates of all other moments of the velocity distribution function are negative, indicating that fluctuations in these moments decay over time scales comparable to the collision time. If perturbations in the form of plane waves with wave vector  $\mathbf{k}$  are applied to a fluid of elastic particles, there are three modes, corresponding to fluctuations in energy and the two momenta transverse to  $\mathbf{k}$  (diffusive modes), which have a real negative growth rate proportional to  $|\mathbf{k}|^2$ , while the density and longitudinal momentum are propagating modes in which the real part is negative and proportional to  $|\mathbf{k}|^2$ , while the imaginary parts are equal in magnitude, opposite in sign and proportional to  $|\mathbf{k}|$ . The behaviour of the hydrodynamic modes for a sheared granular flow turn out to be qualitatively different (Kumaran 2001*a, b*). Since energy is not a conserved variable, there are only four hydrodynamic modes. Moreover, since the shear flow is anisotropic, the magnitudes of the growth rates depend on the direction of the wave vector. For perturbations in the flow direction, there are three longitudinal modes which have a growth rate proportional to  $|\mathbf{k}|^{2/3}$ , where  $k$  is the wavenumber. Of these, two are propagating and one is diffusive. The behaviour of the hydrodynamic modes in the gradient direction is similar to that for an elastic fluid. In the vorticity direction, there are two stable and two unstable modes, and the growth rates of these modes are proportional to  $m$ , where  $m$  is the wave vector in the vorticity direction. In addition, the growth rates of the hydrodynamic modes in the vorticity direction are not adequately captured by the generalized Navier–Stokes equations for granular flows, and it is necessary to include higher moments in order to capture the growth of these perturbations accurately.

There are two objectives of the linear stability analysis carried out here, the first of which is to obtain analytical expressions for the growth rates of the hydrodynamic modes in the long-wave limit, and the second is to examine whether there is a

qualitative difference between the predictions of the Navier–Stokes, Burnett and super-Burnett approximations. Although previous studies have shown that the flow is unstable in the flow and vorticity directions, it is of interest to examine whether analytical expressions for the growth rate can be obtained in the limit of small wavenumber, similar to those obtained in the hydrodynamics of elastic fluids. In the molecular hydrodynamics of simple fluids, analytical solutions for the growth rate can be used to obtain relations between the response function for an external perturbation and the correlation functions for spontaneous fluctuations at equilibrium. In a dissipative system, there is no equipartition theorem which provides the amplitude of fluctuations at equilibrium. However, analytical expressions for the growth rate can be used to obtain relations between the response to external perturbations and the viscometric functions, thereby making it possible to determine the viscometric functions from the response functions in situations where the viscometric functions cannot be easily determined from first principles. In addition, it is easy to evaluate the adequacy of the generalized Navier–Stokes equations for capturing the qualitative behaviour of the growth rates.

The constitutive relations derived in §2 are used to determine the growth rates of the hydrodynamic modes in §§4, 5 and 6. Analytical results are obtained for the growth rate as a function of the viscometric coefficients, and these are evaluated in the limits of low density and near close packing. The viscometric coefficients at intermediate densities depend on the pair distribution function of the particles at contact, and it is necessary to make an assumption about the form of the pair distribution function in order to numerically evaluate the growth rates. The pair distribution function will, in general, be affected by the mean shear, but in the present analysis we assume a strain-rate-independent form for the pair distribution function. This is accurate at low volume fraction, where there are no packing constraints and the pair distribution function is 1, and near close packing, where the pair distribution function is determined predominantly by packing constraints. Since the pair distribution function diverges near close packing, it is not necessary to use a specific form of the pair distribution function in order to obtain analytical results, and it is sufficient to retain the highest power of the pair distribution function (or its derivative with respect to density) in the equation for the growth rate. However, it is necessary to use a specific form of the pair distribution function to obtain numerical results at intermediate volume fractions. Two forms of the pair distribution function are used in the present calculation, the Carnahan–Starling pair distribution function which is accurate at low and moderate densities, and the high-density pair distribution function which is accurate near close packing.

The analysis in §§4, 5 and 6 is restricted to the limit where the length scale is large compared to the conduction length, or  $L \gg \lambda/(1-e)^{1/2}$ . When the length scale is small compared to the conduction length, the energy is a conserved variable, and the system is identical to a gas of elastic hard spheres in the leading approximation when an asymptotic expansion in the parameter  $\epsilon = (1-e)^{1/2}$  is carried out. In this case, the Navier–Stokes mass, momentum and energy equations are adequate to describe the dynamics of the system accurately, and it is known that perturbations are stable in this limit. There are five hydrodynamic modes in this case, two of which are propagating (corresponding to density and longitudinal momentum fluctuations), and three are diffusive (corresponding to energy and two transverse momentum fluctuations). Therefore, as the wavelength or perturbations is decreased from  $L \gg \lambda/(1-e)^{1/2}$  to  $L \ll \lambda/(1-e)^{1/2}$ , a transition is expected from the mode structure in §§4, 5 and 6 for an adiabatic system to the mode structure for a gas of elastic

particles. This transition is examined in detail in §7 for a dilute system in the limit of small  $\epsilon$ .

## 2. Constitutive relation

The system consists of smooth inelastic particles of diameter  $d$  and normal coefficient of restitution  $e$  subject to a mean flow, in which the rate of deformation tensor is given by  $(\partial u_i / \partial x_j) = G_{ij}$ . The mass and diameter of the particles are set equal to 1, so that mass and length dimensions in all dynamical variables are scaled by the particle mass and diameter. However, there is no suitable combination of material properties for scaling time, and the time scale is set by the rate of deformation of the material.

In kinetic theory, the velocity distribution function  $f(\mathbf{c}, \mathbf{x}, t)$  of a gas of inelastic particles is determined by solving the Boltzmann equation, and the stress tensor is determined from the moments of the distribution function. The Boltzmann equation for the distribution function  $f(\mathbf{c}, \mathbf{x}, t)$  is (Chapman & Cowling 1970)

$$\frac{D(\rho f)}{Dt} + \frac{\partial(\rho c_i f)}{\partial x_i} + \left( a_i - \frac{Du_i}{Dt} \right) \frac{\partial(\rho f)}{\partial c_i} - G_{ij} c_j \frac{\partial(\rho f)}{\partial x_i} = \frac{\partial_c(\rho f)}{\partial t}, \quad (2)$$

where  $u_i$  is the mean velocity,  $c_i$  is the difference between the particle velocity and the mean velocity,  $a_i$  is the particle acceleration due to body forces,  $\rho$  is the number density of particles,  $(D/Dt) \equiv (\partial/\partial t) + u_i(\partial/\partial x_i)$  is the substantial derivative, indicial notation is used to represent vectors and a repeated index indicates a scalar product. The distribution function  $f(\mathbf{c}, \mathbf{x}, t)$  is defined such that  $f(\mathbf{c}, \mathbf{x}, t) d\mathbf{c} d\mathbf{x}$  is the probability of finding a particle in the volume  $d\mathbf{c}$  in velocity space and  $d\mathbf{x}$  in real space at time  $t$ . The second and third terms on the left-hand side of (2) are the rates of change of the distribution function due to convective transport in real and velocity space, the fourth term on the left-hand side is due to the motion of particles across streamlines in the flow, and the term on the right-hand side is the collision integral which provides the change in the distribution function due to particle collisions. The collision integral is usually determined assuming that there is no correlation in the velocities of the colliding particles prior to collision (molecular chaos approximation). The collision integral for inelastic particles is

$$\begin{aligned} \frac{\partial_c(\rho f)}{\partial t} = & \chi(\phi) \rho(\mathbf{x}) \rho(\mathbf{x}^*) \int_{\mathbf{c}'} \int_{\mathbf{c}^*} \left( \frac{1}{e^2} f(\mathbf{c}', \mathbf{x}) f(\mathbf{c}^*, \mathbf{x}^*) - f(\mathbf{c}, \mathbf{x}) f(\mathbf{c}^*, \mathbf{x}^*) \right) \\ & \times ((\mathbf{u} + \mathbf{c} - \mathbf{u}^* - \mathbf{c}^*) \cdot \mathbf{k}) \end{aligned} \quad (3)$$

where  $\mathbf{c} + \mathbf{u}(\mathbf{x})$  and  $\mathbf{c}^* + \mathbf{u}(\mathbf{x}^*)$  are the absolute particle velocities,  $\mathbf{c}'$  and  $\mathbf{c}^*$  are the post-collisional fluctuating velocities of a pair of particles with pre-collisional velocities  $\mathbf{c}$  and  $\mathbf{c}^*$ ,  $\mathbf{k}$  is the unit vector along the line from the centre of the particle with velocity  $\mathbf{c}$  to the centre of the particle with velocity  $\mathbf{c}^*$ ,  $\mathbf{x}^* = \mathbf{x} + \mathbf{k}$  is the centre of the particle with velocity  $\mathbf{c}^*$ , the integral is carried out over  $(\mathbf{c} + \mathbf{u} - \mathbf{c}^* - \mathbf{u}^*) \cdot \mathbf{k} > 0$ , and  $\chi(\phi)$  is the pair distribution function which is a function of the volume fraction  $\phi$  of the particles. The factor  $(1/e^2)$  in the first term on the right-hand side of (3) accounts for the contraction in phase space due to a decrease in the kinetic energy in an inelastic collision. The Boltzmann equation is a nonlinear integro-differential equation, and is difficult to solve in general. However, a solution can be obtained when the coefficient of restitution is close to 1 ( $(1-e) \ll 1$ ), so that the dissipation of energy in a collision is small compared to the energy of a particle. In this case, the shear production and



dissipation are neglected in the leading approximation, and the distribution function is a Maxwell–Boltzmann distribution. However, the ‘temperature’ is not determined from external thermodynamic constraints, but from a balance between the source of energy due to the mean shear and the dissipation due to inelastic collisions.

The ‘temperature’ in the Maxwell–Boltzmann distribution is not isotropic, in general, owing to the anisotropy induced by the mean shear. In the present analysis, the anisotropy is included using a distribution function of the form

$$f(\mathbf{c}, \mathbf{x}, t) = \frac{1}{(2\pi)^{3/2} \text{Det}(\mathbf{T})^{1/2}} \exp\left(\frac{-c_i T_{ij}^{-1} c_j}{2}\right), \quad (4)$$

where  $T_{ij} = \langle c_i c_j \rangle$  is a second-order symmetric tensor, and the ensemble average  $\langle c_i c_j \rangle$  is defined as

$$\langle c_i c_j \rangle = \int d\mathbf{c} f(\mathbf{c}, \mathbf{x}, t) c_i c_j. \quad (5)$$

The terms in the matrix  $T_{ij}$  are determined from the balance equation for the second moment  $\rho \langle c_i c_j \rangle$  of the velocity distribution. As explained in §1, we use the adiabatic approximation that the length scale for conduction is small compared to the length scale for the variation of the mean flow,  $L$ , so that there is a local balance between the source of energy due to mean shear and the dissipation of energy due to inelastic collisions. In this case, the second moment equation reduces to

$$\rho \frac{DT_{ij}}{Dt} + \rho(G_{ik} T_{kj} + G_{jk} T_{ki}) = \frac{\partial_c \rho \langle c_i c_j \rangle}{\partial t}. \quad (6)$$

The collisional rate of change of the second moment,  $\langle c_i c_j \rangle$ , is difficult to calculate in general, owing to the nonlinear nature of the Boltzmann collision integral. However, an asymptotic expansion can be used in the parameter  $\epsilon = (1-e)^{1/2}$ , about an isotropic Maxwell–Boltzmann distribution,

$$T_{ij} = \delta_{ij} T + \epsilon T_{ij}^{(1)} + \epsilon^2 T_{ij}^{(2)} + \dots, \quad (7)$$

where it can be assumed, without loss of generality, that  $T_{ii}^{(1)} = T_{ii}^{(2)} = 0$ .

It is useful, at this stage, to discuss the magnitudes of the terms in the expansion for  $T_{ij}$  which are evaluated a little later, in order to analyse the reason for assuming that the leading-order correction is  $O(\epsilon)$ . If  $S = (S_{ij} S_{ji})^{1/2}$  is the magnitude of the symmetric traceless part  $S_{ij} = (G_{ij} + G_{ji} - (2/3)\delta_{ij} G_{kk})/2$ , the results of the analysis (A 4, A 12 and A 18 below) indicate that the scalings for  $T$ ,  $T_{ij}^{(1)}$  and  $T_{ij}^{(2)}$  are as follows,

$$\begin{aligned} T &\sim (G_{ii}/\epsilon^2)^2 \quad \text{for } G_{ii} \gg (\epsilon S) \\ &\sim (S/\epsilon)^2 \quad \text{for } G_{ii} \ll (\epsilon S), \end{aligned} \quad (8)$$

$$\begin{aligned} |T_{ij}^{(1)}| &\sim (T^{1/2} S/\epsilon) \\ &\sim (G_{ii} S/\epsilon^3) \quad \text{for } G_{ii} \gg (\epsilon S) \\ &\sim (S/\epsilon)^2 \quad \text{for } G_{ii} \ll (\epsilon S), \end{aligned} \quad (9)$$

$$\begin{aligned} |T_{ij}^{(2)}| &\sim (S G_{ii}/\epsilon^2) \quad \text{for } G_{ii} \gg (\epsilon S) \\ &\sim (S/\epsilon)^2 \quad \text{for } G_{ii} \ll (\epsilon S). \end{aligned} \quad (10)$$

Thus, the results indicate that the scaling of the mean square velocity is sensitively dependent on the ratio of the isotropic and the symmetric traceless part of the rate of deformation tensor. For a flow without any radial expansion or compression

( $G_{ii} = 0$ ),  $T$ ,  $T_{ij}^{(1)}$  and  $T_{ij}^{(2)}$  are of the same magnitude. For a flow with radial expansion or compression ( $G_{ii} \neq 0$ ),  $|T_{ij}^{(1)}| \sim \epsilon T$ , and  $|T_{ij}^{(2)}| \sim \epsilon^2 T$ . Thus, the second and third terms in (7) are  $O(\epsilon)$  and  $O(\epsilon^2)$  smaller than the first terms for  $\epsilon S \gg G_{ii}$ , and  $O(\epsilon^2)$  and  $O(\epsilon^4)$  smaller than the first term for  $\epsilon S \ll G_{ii}$ .

The procedure used for calculating the collision integral is discussed in detail, since it is useful for anticipating the nature of the terms that appear in the collision integral for the second moments. The change in a function  $\psi(\mathbf{c})$  of the fluctuating velocity during a collision can be written as

$$\frac{\partial \langle \psi(\mathbf{c}) \rangle}{\partial t} = \chi(\phi) \rho(\mathbf{x}^*) \int_{\mathbf{k}} \int_{\mathbf{c}^*} \int_{\mathbf{c}} f(\mathbf{x}, \mathbf{c}) f(\mathbf{x}^*, \mathbf{c}^*) (\psi(\mathbf{c}') - \psi(\mathbf{c})) ((\mathbf{u} + \mathbf{c} - \mathbf{u}^* - \mathbf{c}^*) \cdot \mathbf{k}), \quad (11)$$

where  $\mathbf{c}'$  is the post-collisional velocity for the particle with pre-collisional velocity  $\mathbf{c}$ . Note that the above integral is evaluated for  $(\mathbf{u} + \mathbf{c} - \mathbf{u}^* - \mathbf{c}^*) \cdot \mathbf{k} > 0$ , so that particles approach each other prior to a collision. The above integral is evaluated by changing the independent variables from the particle velocities  $\mathbf{c}$  and  $\mathbf{c}^*$  to the velocity of the centre of mass  $\mathbf{v}$  and the velocity difference  $\mathbf{w}$ ,

$$\begin{aligned} v_i &= (c_i + c_i^* + u_i + u_i^*)/2 \\ &= (c_i + c_i^*)/2 + G_{ij} k_j / 2, \end{aligned} \quad (12)$$

$$\begin{aligned} w_i &= (u_i + c_i - u_i^* - c_i^*) \\ &= (c_i - c_i^*) - G_{ij} k_j. \end{aligned} \quad (13)$$

The velocity of the centre of mass is not altered due to the collision, while the velocity difference after collision  $w'_i$  is related to the velocity difference before collision  $w_i$  by

$$w'_i = (\delta_{ij} - (1 + e)k_i k_j) w_j. \quad (14)$$

The distribution functions  $f(\mathbf{x}, \mathbf{u})$  and  $f(\mathbf{x}^*, \mathbf{u}^*)$  and the variables  $\psi(\mathbf{c})$  and  $\psi(\mathbf{c}')$  are expressed in terms of  $\mathbf{v}$ ,  $\mathbf{w}$  and  $\mathbf{w}'$  using (12), (13) and (14). It is easily verified, that the second terms on the right-hand sides in (12) and (13) are  $O(\epsilon)$  smaller than the first terms on the right-hand sides for a flow with no radial expansion or contraction, and  $O(\epsilon^2)$  smaller than the first terms for a flow with radial expansion or contraction. Therefore, an asymptotic expansion in the parameter  $\epsilon$  is used to evaluate the integral in (11) to the desired accuracy. The details of the calculation are given in Appendix A, and the resulting equation for the stress tensor, correct to  $\epsilon^2$ , is

$$\begin{aligned} \sigma_{ij} &= -p(\phi, S_{ij}, G_{ii}) \delta_{ij} + 2\mu(\phi, S_{ij} G_{ii}) S_{ij} + \mu_b(\phi, S_{ij}, G_{ii}) \delta_{ij} G_{kk} \\ &+ \mathcal{A}(\phi) S_{ik} S_{kj} + \mathcal{B}(\phi) \delta_{ij} S_{kl} S_{lk} + \mathcal{C}(\phi) \delta_{ij} G_{kk}^2 + \mathcal{D}(\phi) S_{ij} G_{kk} \\ &+ \mathcal{E}(\phi) (A_{ik} S_{kj} + A_{jk} S_{ki}) + \mathcal{F}(\phi) (A_{ik} A_{kj} - (\delta_{ij}/3) A_{kl} A_{lk}) \\ &+ \mathcal{G}(\phi) \left( \frac{\partial}{\partial x_i} \left( \frac{1}{\rho} \frac{\partial p}{\partial x_j} \right) + \frac{\partial}{\partial x_j} \left( \frac{1}{\rho} \frac{\partial p}{\partial x_i} \right) - \frac{2\delta_{ij}}{3} \frac{\partial}{\partial x_k} \left( \frac{1}{\rho} \frac{\partial p}{\partial x_k} \right) \right), \end{aligned} \quad (15)$$

where  $p(\phi, T)$ ,  $\mu(\phi, T)$  and  $\mu_b(\phi, T)$  are given by (A 14)–(A 16), and  $\mathcal{A}$  to  $\mathcal{F}$  are given in (A 29) in Appendix A. The first three terms on the right-hand side in (15) are usually included in the Navier–Stokes approximation for the granular flow, which assumes that the stress is given by the usual Newtonian form, but where the viscosity and pressure are functions of the granular temperature. The granular temperature is determined by a balance between the source of energy due to the mean shear and the

dissipation due to inelastic collisions. The last seven terms on the right-hand side of (15) are usually included in the Burnett equations in the kinetic theory of gases. The equation for the temperature  $T$  is given by (A 13),

$$\rho C_v \frac{DT}{Dt} + p(\phi, T)G_{ii} - 2\mu(\phi, T)S_{ik}S_{ki} - \mu_b(\phi, T)G_{ii}^2 + \epsilon^2 R(\phi)T^{3/2} = 0, \quad (16)$$

where  $R(\phi)$  is given by equation (A 17).

It is useful to examine the limiting behaviour of the viscometric coefficients in the limit of low density ( $\phi \rightarrow 0$ ) and near close packing ( $\phi \rightarrow \phi_c$ ). The limiting behaviour of the pressure and the viscosity depend on the strain rate, due to the temperature dependence on the strain rate, and have the form

$$p^{(l)} = \frac{6\phi T^{(l)}}{\pi}, \quad p^{(c)} = \frac{24\phi^2 \chi T^{(c)}}{\pi}, \quad (17)$$

$$\mu^{(l)} = \frac{5\sqrt{T^{(l)}}}{16\sqrt{\pi}}, \quad \mu^{(c)} = \frac{4\phi^2 \chi (12 + \pi)\sqrt{T^{(c)}}}{5\pi^{3/2}}, \quad (18)$$

$$\mu_b^{(l)} = \frac{16\phi^2 \sqrt{T^{(l)}}}{\pi^{3/2}}, \quad \mu_b^{(c)} = \frac{16\phi^2 \chi \sqrt{T^{(c)}}}{\pi^{3/2}}, \quad (19)$$

where  $T^{(l)}$  and  $T^{(c)}$  are the values of  $T$  at low density and near close packing, respectively. The coefficients  $\mathcal{A}$ – $\mathcal{G}$  depend only on density, and have the following leading-order behaviour in the limit  $\phi \rightarrow 0$  (denoted by the superscript  $(l)$ ) and in the limit  $\phi \rightarrow \phi_c$  (indicated by the superscript  $(c)$ ),

$$\mathcal{A}^{(l)}(\phi) = -\frac{125}{5376\phi}, \quad \mathcal{A}^{(c)}(\phi) = \phi_c^2 \chi(\phi) \left( \frac{4}{35} - \frac{192}{35\pi} \right), \quad (20)$$

$$\mathcal{B}^{(l)}(\phi) = \frac{125}{16128\phi}, \quad \mathcal{B}^{(c)}(\phi) = \phi_c^2 \chi(\phi) \left( \frac{9}{70} - \frac{32}{105\pi} \right), \quad (21)$$

$$\mathcal{C}^{(l)}(\phi) = -\frac{4\phi^2}{3}, \quad \mathcal{C}^{(c)}(\phi) = -\frac{4\phi_c^2 \chi(\phi)}{3}, \quad (22)$$

$$\mathcal{D}^{(l)}(\phi) = -\frac{25}{1152\phi}, \quad \mathcal{D}^{(c)}(\phi) = -\phi_c^2 \chi(\phi) \left( \frac{13}{45} + \frac{8}{5\pi} \right), \quad (23)$$

$$\mathcal{E}^{(l)}(\phi) = -\frac{25}{768\phi}, \quad \mathcal{E}^{(c)}(\phi) = -\frac{\phi_c}{12}, \quad (24)$$

$$\mathcal{F}^{(l)}(\phi) = \frac{25}{768\phi}, \quad \mathcal{F}^{(c)}(\phi) = \frac{\phi_c}{12}, \quad (25)$$

$$\mathcal{G}^{(l)}(\phi) = \frac{25}{1536\phi}, \quad \mathcal{G}^{(c)}(\phi) = \frac{\phi_c}{24}. \quad (26)$$

A natural reference point for validating the present results is the Chapman–Enskog theory for dense gases, where the pressure and viscosity are calculated as a function of density in the Navier–Stokes approximation, and the theory for dilute gases where the Burnett coefficients are calculated in the dilute limit. Here, the asymptotic analysis is carried out by expressing the distribution function as a product of the Maxwell–Boltzmann distribution and a Sonine polynomial series in the particle velocities, and the accuracy of the results depends on the number of terms retained in the polynomial expansion. The first-order results, obtained by retaining just the first term in the Sonine polynomial series, are numerically accurate to within 1.4% of more exact results obtained when higher-order terms are retained. In the present calculation,

(A 14) is identical to the result for the pressure in the Chapman–Enskog theory of dense gases if the temperature is considered a thermodynamic variable. Equations (A 15) and (A 16) for the shear and bulk viscosities are identical to those derived using the Chapman–Enskog procedure, when the Sonine polynomial expansion is truncated at the first term. A more accurate expansion, where the higher-order terms are included in the expansion, results in a difference of about 1.4% in the expression for the shear viscosity. The coefficients  $\mathcal{A}^{(l)}$ – $\mathcal{G}^{(l)}$  are identical to those obtained from the Chapman–Enskog theory for dilute gases if the Sonine polynomial expansion for the distribution function is truncated at the first term. The coefficients  $\mathcal{D}^{(l)}$ ,  $\mathcal{E}^{(l)}$ ,  $\mathcal{F}^{(l)}$  and  $\mathcal{G}^{(l)}$  differ by 1.4% from coefficients obtained by including the higher-order terms in the expansion, while the coefficients  $\mathcal{A}^{(l)}$  and  $\mathcal{B}^{(l)}$  differ by about 6.5% from those obtained from a more exact calculation using higher-order terms in the expansion. The Chapman–Enskog theory predicts that  $\mathcal{C}$  is identically zero, which is in agreement with the present result which indicates that the contribution to  $\mathcal{C}$  proportional to  $(1/\phi)$  is identically zero. Thus, the present viscometric coefficients in the Navier–Stokes approximation are close to those obtained in the Chapman–Enskog theory of dense gases, and those in the Burnett approximation are close to those obtained in the dilute limit. The advantage of the present formulation is that results for the Burnett approximation are not restricted to the low-density limit.

In the present calculation, the effect of the super-Burnett terms on the growth rates of the hydrodynamic modes are also examined. There are two types of super-Burnett terms, (i) those analogous to the term proportional to  $\mathcal{G}$  in (15) which contain the higher spatial derivatives of the stress tensor, and (ii) those analogous to the terms proportional to  $\mathcal{A}$  to  $\mathcal{F}$ , which are cubic functions of the strain rate. The terms which contain higher spatial gradients are not significant in the low-wavenumber limit, since they result in higher powers of the wavenumber. However, they could be important in the long-time limit owing to the dependence of the wave vector on time. This issue is discussed in detail in §4.2. The effect of the terms which are cubic functions of the rate of deformation tensor are examined using a stress tensor of the form

$$\begin{aligned}
\sigma_{ij} = & -p(\phi, S_{ij}, G_{ii})\delta_{ij} + 2\mu(\phi, S_{ij}G_{ii})S_{ij} + \mu_b(\phi, S_{ij}, G_{ii})\delta_{ij}G_{kk} \\
& + \mathcal{A}(\phi)S_{ik}S_{kj} + \mathcal{B}(\phi)\delta_{ij}S_{kl}S_{lk} + \mathcal{C}(\phi)\delta_{ij}G_{kk}^2 \\
& + \mathcal{D}(\phi)S_{ij}G_{kk} + \mathcal{E}(\phi)(A_{ik}S_{kj} + A_{jk}S_{ki}) + \mathcal{F}(\phi)(A_{ik}A_{kj} - (\delta_{ij}/3)A_{kl}A_{lk}) \\
& + \mathcal{G}(\phi)\left(\frac{\partial}{\partial x_i}\left(\frac{1}{\rho}\frac{\partial p}{\partial x_j}\right) + \frac{\partial}{\partial x_j}\left(\frac{1}{\rho}\frac{\partial p}{\partial x_i}\right) - \frac{2\delta_{ij}}{3}\frac{\partial}{\partial x_k}\left(\frac{1}{\rho}\frac{\partial p}{\partial x_k}\right)\right) \\
& + \mathcal{H}S_{ik}S_{kl}S_{lj} + \mathcal{I}S_{ik}S_{kj}G_{ll} + \mathcal{J}S_{ij}G_{ll}^2 \\
& + \delta_{ij}(\mathcal{K}S_{kl}S_{lm}S_{mk} + \mathcal{L}S_{kl}S_{lk}G_{mm} + \mathcal{M}G_{kk}^3) + \mathcal{N}A_{ik}A_{kj}G_{ll} \\
& + \mathcal{O}(A_{ik}S_{kj} + A_{jk}S_{ki})G_{ll} + \mathcal{P}S_{ij}A_{kl}A_{lk} + \mathcal{Q}(A_{ik}A_{kl}S_{ij} + S_{ik}S_{kl}A_{lj}) + \mathcal{R}A_{ik}S_{kl}A_{jl} \\
& + \delta_{ij}(\mathcal{S}A_{kl}A_{lk}G_{mm} + \mathcal{T}(S_{kl}A_{lm}A_{mk} + A_{kl}A_{lm}S_{mk})) + \mathcal{U}A_{kl}S_{lm}A_{mk}. \tag{27}
\end{aligned}$$

From dimensional analysis, it can be inferred that the coefficients  $\mathcal{H}$  to  $\mathcal{U}$  are proportional to  $T^{-1/2}$ .

The major difference between the present analysis and the earlier ones of Savage (1992), Babic (1993) and Schmid & Kytomaa (1994) is that the Burnett terms are included in the equation for stress, (15), and the adequacy of this approximation is tested by comparing the results with those obtained by an augmented stress equation which contains the super-Burnett terms, (27). In addition, the conduction term is not

included in the energy equation, since it is small compared to the energy dissipation term when the length scale is larger than the conduction length. The validity of this assumption is checked in §7 for a dilute shear flow, where the hydrodynamic modes are analysed by incorporating the conduction term in the energy equation as well as the Burnett terms in the momentum equation. It is verified that the conduction terms are small when the length scale is larger than the conduction length.

### 3. Linear analysis

In order to compare the predictions of the different models, the growth rates of the hydrodynamic (mass and momentum density) modes are analysed in the limits of high and low density for:

(i) the asymptotic result for the stress tensor correct to second order in  $\epsilon$  given in (15), referred to as the Burnett approximation;

(ii) the asymptotic result for the stress tensor correct to first order in  $\epsilon$ , which corresponds to (15) with  $\mathcal{A}$  to  $\mathcal{G}$  set equal to zero, referred to as the Navier–Stokes approximation; and

(iii) the expression for the stress tensor correct to third order given in (27), with unknown forms of the coefficients  $\mathcal{H}$  to  $\mathcal{U}$ , referred to as the super-Burnett approximation.

The mean velocity is a linear shear flow,

$$\left. \begin{aligned} \bar{u}_x &= \bar{G}y, \\ \bar{u}_y &= 0, \\ \bar{u}_z &= 0, \end{aligned} \right\} \quad (28)$$

where  $\bar{G}$  is assumed to be positive without loss of generality. The mean temperature in this case is given by  $\bar{T} = (\bar{G}^2 \bar{N} / 2\epsilon^2)$ , where  $\bar{N} = N(\bar{\phi})$ , and  $N(\phi)$  is given in equation (A 19). In the low-density limit, the mean temperature is

$$\bar{T}^{(l)} = \frac{5\pi\bar{G}^2}{2304\epsilon^2\phi^2}, \quad (29)$$

and as the density approaches the close-packing density ( $\phi \rightarrow \phi_c$ ), the temperature is

$$\bar{T}^{(c)} = \frac{\bar{G}^2}{\epsilon^2} \left( \frac{1}{15} + \frac{\pi}{180} \right). \quad (30)$$

Conservation equations are written for the particle number density and the velocity fields in the three directions,

$$\partial_t \rho + \partial_i(\rho u_i) = 0, \quad (31)$$

$$\rho(\partial_t u_i + u_j \partial_j u_i) = \partial_j \sigma_{ij}, \quad (32)$$

where  $\partial_t = (\partial/\partial t)$ ,  $\partial_i = (\partial/\partial x_i)$ , and indicial notation is used to represent the components of a vector. The equation for  $T$  is given by (16). The equations for the velocity perturbations are expressed in terms of Fourier modes,

$$\left. \begin{aligned} \rho(x, y, z, t) &= \bar{\rho} + \check{\rho}(t) \exp(ikx + ily + imz), \\ u_x(x, y, z, t) &= \bar{u}_x + \check{u}_x(t) \exp(ikx + ily + imz), \\ u_y(x, y, z, t) &= \check{u}_y(t) \exp(ikx + ily + imz), \\ u_z(x, y, z, t) &= \check{u}_z(t) \exp(ikx + ily + imz), \\ T(x, y, z, t) &= \bar{T} + \check{T} \exp(ikx + ily + imz) \end{aligned} \right\}. \quad (33)$$

When the above perturbations are inserted into the mass and momentum equations, the resultant equations are explicitly dependent on the  $y$ -coordinate due to the  $y$ -dependent mean flow if the wave vectors are independent of time. For example, in the linearized mass conservation equation,

$$\partial_t \tilde{\rho} + ik\bar{G}y\partial_x \tilde{\rho} + \bar{\rho}(iku_x + ilu_y + imu_z) = 0, \quad (34)$$

the second term on the left-hand side depends explicitly on the  $y$ -coordinate. In order to avoid the presence of terms that depend explicitly on the  $y$ -coordinate, it is necessary to assume that the wave vectors are time dependent and ‘turn’ with the mean flow (Savage 1992). The wave vectors are chosen to be

$$\left. \begin{aligned} k(t) &= k_0, \\ l(t) &= l_0 - \bar{G}tk_0, \\ m(t) &= m_0. \end{aligned} \right\} \quad (35)$$

With this assumption, the mass conservation equation reduces to

$$\partial_t \tilde{\rho} + \bar{\rho}(iku_x + ilu_y + imu_z) = 0. \quad (36)$$

However, this results in wave vectors that are explicitly dependent on time, and the growth of the perturbations has to be determined by iterative integration for perturbations with  $k_0 \neq 0$ . When these expressions are inserted into (31) and (32), and linearized in the perturbations to the density and velocity, we obtain the equations for the hydrodynamic modes,

$$\partial_t \tilde{\rho} + \bar{\rho}(ik\tilde{u}_x + il\tilde{u}_y + im\tilde{u}_z) = 0, \quad (37)$$

$$\bar{\rho}\partial_t \tilde{u}_x + \bar{G}\tilde{u}_y = ik\tilde{\sigma}_{xx} + il\tilde{\sigma}_{xy} + im\tilde{\sigma}_{xz}, \quad (38)$$

$$\bar{\rho}\partial_t \tilde{u}_y = ik\tilde{\sigma}_{yx} + il\tilde{\sigma}_{yy} + im\tilde{\sigma}_{yx}, \quad (39)$$

$$\bar{\rho}\partial_t \tilde{u}_z = ik\tilde{\sigma}_{zx} + il\tilde{\sigma}_{zy} + im\tilde{\sigma}_{zx}. \quad (40)$$

The equation for  $T$ , (16), has the form

$$\begin{aligned} \bar{\rho}C_v\partial_t \tilde{T} + \bar{p}i(k\tilde{u}_x + l\tilde{u}_y + m\tilde{u}_z) - 2\bar{\mu}\bar{G}i(l\tilde{u}_x + k\tilde{u}_y) - \bar{G}^2\bar{\mu}_\rho\tilde{\rho} \\ + \frac{3\epsilon^2\bar{R}\bar{T}^{1/2}\tilde{T}}{2} + \epsilon^2\bar{T}^{3/2}\bar{R}_\rho\tilde{\rho} = 0 \end{aligned} \quad (41)$$

where  $\bar{R} = R(\bar{\phi})$  and  $\bar{R}_\rho = (dR(\phi)/d\rho)|_{\phi=\bar{\phi}}$ .

The mass and momentum equations contain terms that depend on the temperature and density perturbations because of the dependence of the pressure and viscosity on the density and the temperature. Since the pressure is proportional to  $T$  and the shear and bulk viscosities are proportional to  $T^{1/2}$ , the corrections to the pressure and viscosity due to variations in the density and the strain rate can be written as

$$\left. \begin{aligned} \tilde{p} &= \bar{p}_\rho\tilde{\rho} + \frac{\bar{p}\tilde{T}}{\bar{T}}, \\ \tilde{\mu} &= \bar{\mu}_\rho\tilde{\rho} + \frac{\bar{\mu}\tilde{T}}{2\bar{T}}, \\ \tilde{\mu}_b &= \bar{\mu}_{b\rho}\tilde{\rho} + \frac{\bar{\mu}_b\tilde{T}}{2\bar{T}} \end{aligned} \right\} \quad (42)$$

where

$$\bar{\cdot}_\rho \equiv \left. \frac{\partial \cdot}{\partial \rho} \right|_{\rho=\bar{\rho}, G_{ij}=\bar{G}_{ij}}. \quad (43)$$

Since the functions  $\mathcal{A}(\phi)$ – $\mathcal{G}(\phi)$  are independent of temperature, the perturbations to these functions are only due to perturbations in the density. The corrections to the functions  $\mathcal{H}$ – $\mathcal{U}$  due to fluctuations in the strain rate are given by

$$\tilde{\mathcal{H}} = \bar{\mathcal{H}}_\rho \tilde{\rho} - \frac{\bar{\mathcal{H}} \bar{T}}{2\bar{T}}, \quad (44)$$

since these are proportional to  $T^{-1/2}$ .

Using (42)–(44), the linearized mass, momentum and energy equations, (37)–(40) can be expressed as

$$\partial_t \begin{pmatrix} \tilde{\rho} \\ \tilde{u}_x \\ \tilde{u}_y \\ \tilde{u}_z \\ \tilde{T} \end{pmatrix} + \mathbf{A} \begin{pmatrix} \tilde{\rho} \\ \tilde{u}_x \\ \tilde{u}_y \\ \tilde{u}_z \\ \tilde{T} \end{pmatrix} = 0, \quad (45)$$

where the elements of the matrix  $\mathbf{A}$  are given in Appendix B. Equation (45) has five solutions for the growth rate. Of these, the growth rate for temperature fluctuations is negative and proportional to  $\epsilon^2$  in the limit of small wavenumber, since energy is not conserved. The growth rates of the other four modes decrease proportional to a power of the wavenumber in this limit. Therefore, (45) can be solved in two ways. The first is to solve for all five growth rates, and examine the wavenumber scaling of the four conserved modes alone. The second is to assume that the relation between the temperature and strain rate fluctuations is given by (A 18), and use this to substitute for the temperature in the density and momentum equations. It was verified that these two approaches provide identical results for the growth rate, and the growth rates obtained in this manner are reported in §§4, 5 and 6.

The matrix  $\mathbf{A}$  can be written as a function of time using the substitution 35 for the wavenumber  $l$ ,

$$\mathbf{A} = \mathbf{A}_0 + t\mathbf{A}_1 + t^2\mathbf{A}_2. \quad (46)$$

It should be noted that the terms in expansion (46) arise from the  $l$ -dependent terms in the elements of the matrix  $\mathbf{A}$ , and the substitution  $l = l_0 - k_0 \bar{G}t$ . Therefore, the highest power of  $t$  in (46) is identical to the highest power of  $l$  in  $\mathbf{A}$ . Equation (45) can be formally solved to obtain

$$\begin{pmatrix} \tilde{\rho}(t) \\ \tilde{u}_x(t) \\ \tilde{u}_y(t) \\ \tilde{u}_z(t) \\ \tilde{T} \end{pmatrix} = \exp(-t\mathbf{A}_0 - (t^2/2)\mathbf{A}_1 - (t^3/3)\mathbf{A}_2) \begin{pmatrix} \tilde{\rho}(0) \\ \tilde{u}_x(0) \\ \tilde{u}_y(0) \\ \tilde{u}_z(0) \\ \tilde{T}(0) \end{pmatrix}. \quad (47)$$

Equation (47) provides the complete solution for the growth of perturbations. In the present study, asymptotic analysis is used to deduce the growth rates in the short- and long-time limit, since these provide the limiting behaviour for the growth of the perturbations. For  $\bar{G}t \ll 1$ , it is expected that the response is linear, and the dominant contribution to the growth rate is due to the first term on the right-hand

side of (46), while for  $\bar{G}t \gg 1$ , the dominant contribution is due to the third term on the right-hand side of (46). It should also be noted that  $\mathbf{A}_1$  and  $\mathbf{A}_2$  are identically zero for perturbations in the gradient–vorticity plane with  $k = 0$ , and the growth of perturbations is exponential. The growth of perturbations in the plane of flow is analysed first, and the short- and long-time behaviour of these modes is obtained. The special cases of perturbations along the gradient and vorticity directions are then considered.

Since most of the results in the present analysis are analytical, it is not necessary to assume a specific form for the pair correlation function  $\chi(\phi)$ , and it is sufficient to note that  $\chi \rightarrow 1$  for  $\phi \rightarrow 0$ , and  $\chi$  diverges for  $\phi \rightarrow \phi_c$ , where  $\phi_c$  is the volume fraction at close packing. In certain cases, numerical results are evaluated in order to determine the volume fraction at which there is a transition from stable to unstable modes. In these cases, results are obtained using the Carnahan–Starling pair distribution function,

$$\chi(\phi) = \frac{2 - \phi}{2(1 - \phi)^3}, \quad (48)$$

which is accurate at low- and moderate-volume fractions, and the high-density pair distribution function,

$$\chi(\phi) = \frac{1}{1 - (\phi/\phi_c)^{1/3}}, \quad (49)$$

which is more accurate as the close packing volume fraction is approached.

#### 4. Perturbations in the plane of flow

Equations (37)–(40) indicate that the growth rates of the hydrodynamic modes are not isotropic, and depend on the direction of the wave vector. For waves in the plane of flow with  $m = 0$ , (B 1) indicates the elements  $\Lambda_{\rho z}$ ,  $\Lambda_{xz}$ ,  $\Lambda_{yz}$ ,  $\Lambda_{Tz}$ ,  $\Lambda_{z\rho}$ ,  $\Lambda_{zx}$ ,  $\Lambda_{zy}$  and  $\Lambda_{zT}$  are zero, and so the equation for the  $z$ -momentum is decoupled from the density,  $x$ - and  $y$ -momentum and energy equations. The  $z$ -momentum equation is solved explicitly to obtain the growth rate of momentum in the vorticity direction, which is given in the Burnett approximation by

$$\left( \frac{\partial}{\partial t} + s_{0z} + s_{1z}t + s_{2z}t^2 \right) \tilde{u}_z = 0, \quad (50)$$

where

$$\left. \begin{aligned} s_{0z} &= \frac{\bar{\mu}}{\bar{\rho}}(k_0^2 + l_0^2) + \frac{k_0 l_0 \bar{G}}{2}(\bar{\mathcal{A}} + \bar{\mathcal{E}}) \\ &\quad + \frac{\bar{G}^2 k_0^2}{\bar{\rho}} \left( \frac{\bar{\mathcal{H}}}{8} - \frac{\bar{\mathcal{P}}}{4} - \frac{\bar{\mathcal{R}}}{8} \right) + \frac{\bar{G}^2 l_0^2}{\bar{\rho}} \left( \frac{\bar{\mathcal{H}}}{8} - \frac{\bar{\mathcal{P}}}{4} - \frac{\bar{\mathcal{Q}}}{4} + \frac{\bar{\mathcal{R}}}{8} \right), \\ s_{1z} &= -2\bar{G}k_0 l_0 \bar{\mu} - \frac{\bar{G}^2 k_0^2}{2}(\bar{\mathcal{A}} + \bar{\mathcal{E}}) - \frac{\bar{G}^3 k_0 l_0}{\bar{\rho}} \left( \frac{\bar{\mathcal{H}}}{4} - \frac{\bar{\mathcal{P}}}{2} - \frac{\bar{\mathcal{Q}}}{2} + \frac{\bar{\mathcal{R}}}{4} \right), \\ s_{2z} &= \frac{\bar{G}^2 k_0^2 \bar{\mu}}{\bar{\rho}} + \frac{\bar{G}^4 k_0^2}{\bar{\rho}} \left( \frac{\bar{\mathcal{H}}}{8} - \frac{\bar{\mathcal{P}}}{4} - \frac{\bar{\mathcal{Q}}}{4} + \frac{\bar{\mathcal{R}}}{8} \right). \end{aligned} \right\} \quad (51)$$

The solution of (50) is

$$\tilde{u}_z(t) = \tilde{u}_z(0) \exp[-(s_{0z}t + (s_{1z}t^2/2) + (s_{2z}t^3/3))]. \quad (52)$$



Since  $s_{0z}$  and  $s_{2z}$  are always positive, perturbations are stable at both early and late times. In the asymptotic limit  $\epsilon \rightarrow 0$ ,  $\bar{\mu}$  is  $O(1/\epsilon)$  larger than  $\bar{\mathcal{A}}\bar{G}$  and  $\bar{\mathcal{E}}\bar{G}$ , and so perturbations are always stable, though the Burnett-order terms have a destabilizing effect on the perturbations (note that  $\bar{\mathcal{A}}$  and  $\bar{\mathcal{E}}$  are negative in the low- and high-density limits). Equation (50) indicates that the dispersion relation for the  $z$ -momentum in the Burnett and super-Burnett approximations have the same form as those in the Navier–Stokes approximation, though there are higher-order corrections for the growth rate proportional to  $k_0 l_0$ .

The growth rates for the other three modes are determined by setting the determinant of the dispersion matrix equal to zero. It is difficult to obtain an analytical solution for the growth rate, so an asymptotic expansion in the wavenumber is used, and the growth of perturbations in the short- and long-time limit are examined in detail.

#### 4.1. Short-time limit

In the short-time limit  $\bar{G}t \ll 1$ , when terms correct to quadratic order in the wavenumber are retained, it is found that the growth of perturbations of the other three conserved modes is proportional to  $\exp(s_{\rho xy} t)$ . The expression for  $s_{\rho xy}$ , correct to quadratic order in the wavenumber, is

$$s_{\rho xy}^3 + k^2 \bar{G}^2 \left( \frac{\epsilon^2 \bar{T}^{3/2} (3\bar{R}\bar{\mu}_\rho - \bar{\mu}\bar{R}_\rho)}{3\bar{R}\epsilon^2 \bar{T}^{3/2} - \bar{G}^2 \bar{\mu}} + \frac{\bar{G}^2}{8} (\bar{\mathcal{H}}_\rho - 2\bar{\mathcal{P}}_\rho - 2\bar{\mathcal{Q}}_\rho + \bar{\mathcal{R}}_\rho) \right. \\ \left. + \frac{\bar{G}^2 \bar{T}}{8} \frac{(\epsilon^2 \bar{R}_\rho \bar{T}^{3/2} - \bar{G}^2 \bar{\mu}_\rho)}{(3\bar{R}\epsilon^2 \bar{T}^{3/2} - \bar{G}^2 \bar{\mu})} (\bar{\mathcal{H}} - 2\bar{\mathcal{P}} - 2\bar{\mathcal{Q}} + \bar{\mathcal{R}}) \right) \\ + \bar{G}kl \left( -\bar{p}_\rho^* + \frac{2\bar{p}(\epsilon^2 \bar{R}_\rho \bar{T}^{3/2} - \bar{G}^2 \bar{\mu}_\rho)}{(3\bar{R}\epsilon^2 \bar{T}^{3/2} - \bar{G}^2 \bar{\mu})} \right) = 0, \quad (53)$$

where  $\bar{p}^*$ , the pressure modified by the Burnett coefficients, is

$$\bar{p}^* = \bar{p} + \bar{G}^2 (-\bar{\mathcal{A}}/4 - \bar{\mathcal{C}}/2 + \bar{\mathcal{E}}/2 + \bar{\mathcal{F}}/12). \quad (54)$$

In the limits of low and high density, (53) reduces to

$$s_{\rho xy}^3 - \bar{G}^3 k_0^2 \frac{5\sqrt{5}\pi}{4608\epsilon\bar{\phi}^2} + \frac{5k_0 l_0 \bar{G}^3 \pi}{2304\epsilon^2 \bar{\phi}^2} = 0, \quad (55)$$

$$s_{\rho xy}^3 + \frac{2k_0^2 \bar{\chi}_\rho \bar{G}^3 \bar{\phi}^2 (12 + \pi)^{3/2}}{15\sqrt{5}\epsilon\pi^{3/2}} - \frac{2k_0 l_0 \bar{\chi}_\rho \bar{G}^3 \bar{\phi}^2 (12 + \pi)}{15\epsilon^2 \pi} = 0. \quad (56)$$

It is apparent that there is no qualitative difference between the predictions of the Navier–Stokes, Burnett and super-Burnett approximations, though there are quantitative differences.

Equation (53) indicates that the growth rate has an unusual  $k_0^{2/3}$  power-law dependence on the wavenumber for  $l_0 = 0$ , and an unusual  $(k_0 l_0)^{1/3}$  dependence for  $l_0 \neq 0$ , and it is instructive to examine the reasons for this. The mass and momentum equations, (37)–(39), correct to leading order in small  $k$  and  $l$ , are

$$s_{\rho xy} \tilde{\rho} + \bar{\rho} i k \tilde{u}_x + \bar{\rho} i l \tilde{u}_y = 0, \quad (57)$$

$$\bar{\rho} (s_{\rho xy} \tilde{u}_x + \bar{G} \tilde{u}_y) + (i k \bar{p}_\rho - i \bar{G} l \bar{\mu}_\rho) \tilde{\rho} + \frac{i}{\bar{T}} (k \bar{p} - \bar{G} l \bar{\mu}) \tilde{T} = 0, \quad (58)$$

$$\bar{\rho} s_{\rho xy} \tilde{u}_y + (i l \bar{p}_\rho - i \bar{G} k \bar{\mu}_\rho) \tilde{\rho} + \frac{i}{\bar{T}} (l \bar{p} - \bar{G} k \bar{\mu}) \tilde{T} = 0. \quad (59)$$

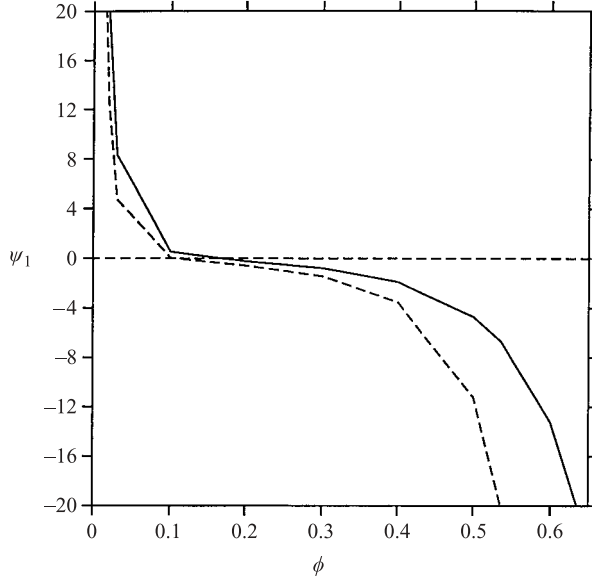


FIGURE 1. Variation of  $\psi_1 = (s_{\rho xy}^3 \epsilon / \bar{G}^3 k_0^2)$  with  $\bar{\phi}$  for  $l_0 = 0$ , where  $s_{\rho xy}$  is given by equation (53). The solid curve is obtained when the Carnahan–Starling approximation (equation (48)) is used for the pair distribution function, and the broken curve is obtained when the high-density approximation (equation (49)) is used for the pair distribution function.

It is apparent that the convection due to the mean flow in the  $x$ -momentum equation (58) is responsible for a coupling between the  $x$ - and  $y$ -momentum equations. This coupling between the  $x$ - and  $y$ -momentum equations, owing to the turning of the wave vector by the mean flow, results in the  $k_0^{2/3}$  scaling for the growth rate.

Equation (53) also indicates that there is a qualitative difference between the growth rates for perturbations in the flow direction with  $l_0 = 0$ , and for transverse perturbations with  $l_0 \neq 0$ . For perturbations in the flow direction, the growth rate is proportional to  $(-1)^{1/3} \bar{G} k_0^{2/3}$ , and there is one diffusive solution with a zero imaginary part, and two propagating solutions with equal real parts and equal and opposite imaginary parts. In the low-density limit,  $s_{\rho xy}^3$  is positive, and so the diffusive mode has a positive real part, indicating that it is unstable, while the propagating modes have negative real parts, indicating that they are stable, in agreement with the low-density analysis of Kumaran (2001*b*). The growth rates scale as  $\bar{G} k_0^{2/3} \epsilon^{-1/3}$ , and this scaling behaviour is also in agreement with the low-density results of Kumaran (2001*b*). When the volume fraction approaches close packing,  $(s_{\rho xy})$  is negative, and the diffusive mode is stable while the propagating modes are unstable. As shown in figure 1, there is an intermediate volume fraction at which  $s_{\rho xy}$  is identically zero, and, at this volume fraction, all three solutions for the growth rate are identically zero, indicating that all modes are neutrally stable. The volume fraction at which the growth rate passes through zero is  $\bar{\phi} = 0.148$  in the Carnahan–Starling approximation, (48), for the pair distribution function, and  $\bar{\phi} = 0.100$  in the high-density approximation (49).

Next, we consider the case  $\bar{p}_\rho k_0 l_0 \gg \bar{G} \bar{\mu}_\rho k_0^2$ , which is equivalent to  $l_0 \gg \epsilon k_0$ , since the viscosity is  $O(\bar{G}/\epsilon)$  while the pressure is  $O(\bar{G}^2/\epsilon^2)$  in the limit  $\epsilon \rightarrow 0$ . The leading-order growth rate (53) is proportional to  $-(-1)^{1/3} \bar{G} k_0^{1/3} l_0^{1/3}$ . There are two

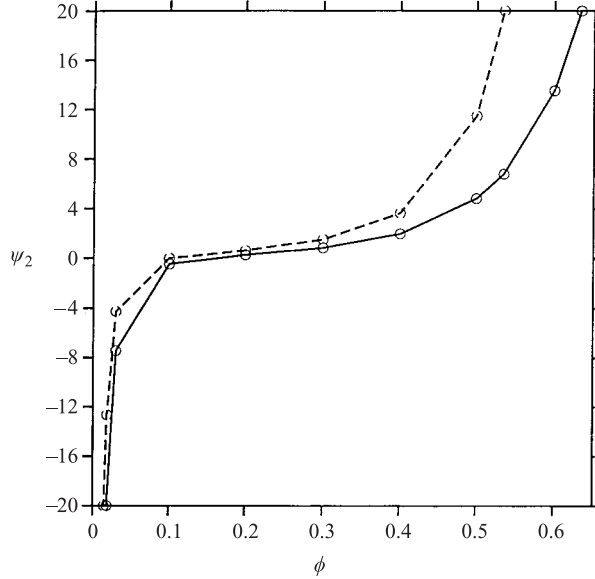


FIGURE 2. Variation of  $\psi_2 = (s_{\rho_{xy}}^3 \epsilon^2 / \bar{G}^3 k_0 l_0)$  with  $\bar{\phi}$  for  $l_0 \gg \epsilon k_0$ , where  $s_{\rho_{xy}}$  is given by equation (53), and  $\psi_2 = -(s_{\rho_z}^2 \epsilon^2 / \bar{G}^2 m^2)$ , where  $s_{\rho_z}'$  is the component of  $s_{\rho_z}$  in equation (71) which is proportional to  $m$ . The solid curve is obtained when the Carnahan–Starling approximation (equation (48)) is used for the pair distribution function, and the broken curve is obtained when the high-density approximation (equation (49)) is used for the pair distribution function.

complex conjugate and one real solutions for the growth rate in this case as well. In the low-density limit, (55) shows that the propagating modes are unstable, while the diffusive mode is stable. Near close packing, (56), shows that the diffusive mode is unstable while the propagating modes are stable in this case. There is an intermediate volume fraction, as shown in figure 2, which is  $\bar{\phi} = 0.149$  in the Carnahan–Starling model, (48), for the pair distribution function and 0.100 in the high-density model, (49), for the pair distribution function, at which the growth rates of all three modes are identically zero. At this point, there is an exchange of stability with the real and imaginary parts of all three solutions passing through zero simultaneously.

#### 4.2. Long-time limit

In the limit of long time  $\bar{G}t \gg 1$ , the term proportional to  $t^2$  on the right-hand side of (46) is dominant. The velocity fluctuations decay as

$$\left. \begin{aligned} \tilde{u}_x(t) &= \exp(-\bar{\mu}^* \bar{G}^2 k_0^2 t^3 / 3) \tilde{u}_x(0), \\ \tilde{u}_y(t) &= \exp(-(\bar{\mu}^* / 3 + \bar{\mu}_b^*) \bar{G}^2 k_0^2 t^3 / 3) \tilde{u}_y(0), \\ \tilde{u}_z(t) &= \exp(-\bar{\mu}^* \bar{G}^2 k_0^2 t^3 / 3) \tilde{u}_z(0). \end{aligned} \right\} \quad (60)$$

where

$$\left. \begin{aligned} \bar{\mu}^* &= \bar{\mu} + \bar{G}^2 (\bar{\mathcal{H}}/8 - \bar{\mathcal{P}}/4 - \bar{\mathcal{Q}}/4 + \bar{\mathcal{R}}/8), \\ \bar{\mu}_b^* &= \bar{\mu}_b + \bar{G}^2 (\bar{\mathcal{H}}/12 + \bar{\mathcal{I}}/4 + \bar{\mathcal{K}}/4 + \bar{\mathcal{L}}/2 - \bar{\mathcal{N}}/4 \\ &\quad - \bar{\mathcal{O}}/2 - \bar{\mathcal{R}}/12 - \bar{\mathcal{S}}/2 - \bar{\mathcal{T}}/6 - \bar{\mathcal{U}}/12). \end{aligned} \right\} \quad (61)$$

are the shear viscosity and bulk viscosity modified by the Burnett and super-Burnett corrections. Equation (60) indicates that the velocity perturbations are stable in the long-time limit, and the decay rate of these perturbations also scales as  $\bar{G}k_0^{2/3}$  in this limit. There is a quantitative variation in the long-time growth rate when the Burnett terms are included, but the qualitative behaviour remains unchanged.

The results in (61) should be interpreted with care, since the super-Burnett analogue of the Burnett term which is proportional to the second spatial gradient of pressure has been neglected. In the super-Burnett approximation, it is expected that there is a term of the type  $(\partial(\rho^{-1}(\partial\sigma_{jk}^{(1)}/\partial x_k))/\partial x_i)$ , where  $\sigma_{jk}^{(1)}$  is the  $O(\epsilon)$  contribution to the stress tensor. It is easy to see that this term results in a factor proportional to  $\exp(Ck_0^4 t^5)$  on the right-hand side of (61), and this term is dominant at late times, where  $C$  is a coefficient that can be determined from the form of the super-Burnett term. The stability then depends on the sign of the real part of  $C$ , which has not been evaluated here. If  $C$  is negative, then the perturbations are stable in the long-time limit. Even though the decay at long times is dominated by the super-Burnett term, it can be shown that the Navier–Stokes approximation provides an accurate estimate of the maximum amplitude of the fluctuations after the transient growth. The growth rate of perturbations at early times is proportional to  $k_0^{2/3}\bar{G}$  from (53), while the decay at long times in the Navier–Stokes approximation is proportional to  $\bar{G}^3 k_0^2 t^2$  from (60). The maximum amplitude is attained when these two are of the same magnitude, or when  $t \sim k_0^{-2/3}\bar{G}^{-1}$ . In this case, the correction to the growth rate due to the Burnett term is  $O(\bar{G}^4 k_0^4 t^4)$ , or  $O(k_0^{4/3})$ , which is small in the small-wavenumber limit. Thus, if the higher-order contributions to the growth rate due to the super-Burnett and higher corrections are stabilizing, the Navier–Stokes approximation is adequate to describe the transient growth of perturbations accurately.

## 5. Perturbations in the gradient direction

Equation (53) indicates that the growth rates for the density and  $x$ - and  $y$ -momentum modes are identically zero for  $k = 0$ . In this case, it is necessary to incorporate corrections to the dispersion relation that are higher order in  $l$ , in order to determine the leading behaviour of the growth rate. The growth rate for the momentum in the  $z$ -direction is still given by (50). Of the other three modes, one is diffusive with real growth rate proportional to  $l^2$ , while the other two are propagating with complex conjugate growth rates in which the imaginary part is proportional to  $l$  and the real part is proportional to  $l^2$ .

### 5.1. Diffusive mode

The growth rate of the diffusive mode is given, in the super-Burnett approximation, by

$$s_d = \frac{-\bar{\mu}^*(\epsilon^2 \bar{T}^{3/2}(3\bar{R}\bar{p}_\rho - 2\bar{p}^*\bar{R}_\rho) + \bar{G}^2(\bar{\mu}^*\bar{p}_\rho^* - 2\bar{p}^*\bar{\mu}_\rho^*))l^2}{\bar{T}^{3/2}\epsilon^2\bar{\rho}(3\bar{R}\bar{p}_\rho^* - 2\bar{p}^*\bar{R}_\rho) + \bar{G}^2(4\bar{\mu}^*\bar{p}^* + \bar{\rho}(2\bar{p}^*\bar{\mu}_\rho^* - \bar{\mu}^*\bar{p}_\rho^*))}, \quad (62)$$

where  $\bar{p}^*$  and  $\bar{\mu}^*$  are given by (54) and (61). Equation (62) indicates that the Burnett and super-Burnett terms alter the quantitative value of the growth rate of the hydrodynamic modes, but do not affect the scaling with wavenumber. In the limit of low density, this growth rate is given by

$$s_d^{(l)} = -\frac{\sqrt{5}\bar{G}\pi}{192\epsilon\phi}l^2, \quad (63)$$

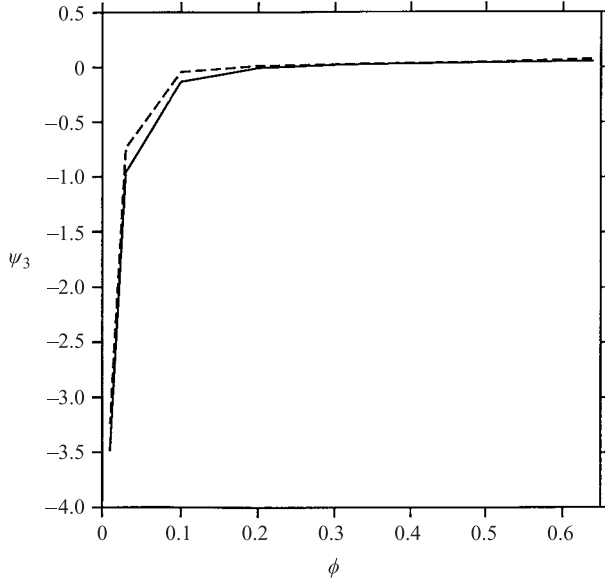


FIGURE 3. Variation of  $\psi_3 = (s_d \epsilon / \bar{G} l^2)$  with  $\bar{\phi}$ , where  $s_d$  is given by equation (62). The solid curve is obtained when the Carnahan–Starling approximation (equation (48)) is used for the pair distribution function, and the broken curve is obtained when the high-density approximation (equation (49)) is used for the pair distribution function.

and this diffusive mode is stable. Near close packing, the growth rate of this diffusive mode is

$$s_d^{(c)} = \frac{(48 - \pi) \bar{G} \bar{\phi}}{360 \epsilon} \left( \frac{12 + \pi}{5\pi} \right)^{1/2} l^2. \quad (64)$$

Equation (64) indicates that the diffusive mode is unstable in the limit of high density, though the growth rate of this mode is low and does not diverge as the system approaches close packing. The growth rate is shown as a function of volume fraction in figure 3 at intermediate densities, and it is found that there is a transition from stable to unstable modes at a volume fraction  $\phi = 0.217$  when the Carnahan–Starling approximation (equation (48)) is used for the pair distribution function, and  $\phi = 0.154$  when the high-density approximation (equation (49)) is used for the pair distribution function. Even though this mode becomes unstable, the magnitude of the growth rate, scaled by  $(\bar{G}/\epsilon)$ , is small, as shown in figure 3.

Since the long-wave analysis indicates that the  $O(l^2)$  contribution to the growth rate is positive, it is necessary to examine the next correction to the growth rate to determine the maximum wavenumber for unstable modes. The calculation of the next higher contribution is algebraically complicated, and so only the results for volume fractions near close packing are provided. In this case, the next correction to the growth rate turns out to be  $O(l^4)$ , and the growth rate has the form

$$s_d = s_d^{(c)} \left( 1 - \frac{(12 + \pi) l^2}{120 \epsilon^2} \right), \quad (65)$$

where  $s_d^{(c)}$  is given in (64). This calculation indicates that perturbations are unstable for  $l < \epsilon(120/(12 + \pi))^{1/2}$ . However, the present analysis is valid for  $l \ll \epsilon$ , since the conduction terms in the energy equation are neglected in comparison to the source

and dissipation of energy, and the result for the maximum wavenumber of unstable modes is not accurate. This is corrected by incorporating the conduction term  $\kappa l^2 \bar{T}$  in the energy equation, where  $\kappa$  is the thermal conductivity. When thermal conductivity is included, it is found that the growth rate, in the leading approximation in small wavenumber, is

$$s_d = s_d^{(c)} \left( 1 - \frac{(12 + \pi)l^2}{120\epsilon^2} \right) - \frac{l^4(12 + \pi)\kappa\pi}{1080\epsilon^2\phi}, \quad (66)$$

instead of (65). Since the thermal conductivity increases proportional to  $\chi$  near close packing, the stabilizing effect of the term proportional to the thermal conductivity in (66) is dominant, and the maximum wavenumber for unstable modes is  $l = (1080\epsilon^2\phi(s_d^{(c)}/l^2)/(\pi(12 + \pi)\kappa))^{1/2}$ . Since the thermal conductivity increases proportional to  $\chi$  near close packing, the maximum wavenumber of unstable modes decreases proportional to  $\chi^{-1/2}$  in this limit.

### 5.2. Propagating modes

The other two solutions are propagating, with negative real parts and equal and opposite imaginary parts. The results are provided only for the Navier–Stokes model, since the results for the Burnett and super-Burnett models are algebraically complicated. It is sufficient to note that the scaling of the growth rate with wavenumber is captured by the Navier–Stokes approximation, and the Burnett and super-Burnett approximations result in quantitative changes in the numerical coefficients of the growth rates. The imaginary part of the propagating growth rates is

$$s_{pi} = \pm i l \left( \bar{p}_\rho + \frac{2\bar{p}}{\rho} \left( \frac{\bar{G}^2(2\bar{\mu} + \bar{\rho}\bar{\mu}_\rho) - \epsilon^2\bar{p}\bar{R}_\rho\bar{T}^{3/2}}{3\bar{R}\epsilon^2\bar{T}^{3/2} - \bar{G}^2\bar{\mu}} \right) \right)^{1/2}, \quad (67)$$

while the real part has the form

$$s_{pr} = l^2 \frac{\bar{\mu}(\epsilon^2\bar{T}^{3/2}(3\bar{R}\bar{p}_\rho - 2\bar{p}\bar{R}_\rho) + \bar{G}^2(\bar{\mu}\bar{p}_\rho - 2\bar{\mu}_\rho\bar{p}))}{2(\bar{\rho}\epsilon^2\bar{T}^{3/2}(3\bar{R}\bar{p}_\rho - 2\bar{p}\bar{R}_\rho) + \bar{G}^2(4\bar{\mu}\bar{p} + \bar{\rho}(2\bar{\mu}_\rho\bar{p} - \bar{\mu}\bar{p}_\rho)))} + \frac{s_{pi}^2}{6} \frac{\epsilon^2\bar{T}^{3/2}\bar{R}(21\bar{\mu} + 9\bar{\mu}_b) + 6\bar{p}^2 + 9\bar{p}_\rho\bar{\rho}^2\bar{T} - \bar{G}^2(\bar{\mu}^2 + 3\bar{\mu}\bar{\mu}_b) + 9\bar{\rho}^2\bar{T}(s_{pi}/l^2)}{6(\bar{\rho}\epsilon^2\bar{T}^{3/2}(3\bar{R}\bar{p}_\rho - 2\bar{p}\bar{R}_\rho) + \bar{G}^2(4\bar{\mu}\bar{p} + \bar{\rho}(2\bar{\mu}_\rho\bar{p} - \bar{\mu}\bar{p}_\rho)))} \quad (68)$$

In the limit of low density, the growth rate of the propagating mode has the form

$$s_p = \frac{\pm i l \sqrt{5\pi}\bar{G}}{48\epsilon\bar{\phi}} - \frac{l^2\sqrt{5}\bar{G}\pi}{2304\epsilon^3\bar{\phi}^2}. \quad (69)$$

Near close packing, the limiting value of the growth rate of the propagating modes are

$$s_p = \pm \frac{i l \bar{G} \phi \sqrt{2\bar{\chi}_\rho \sqrt{12 + \pi}}}{\epsilon \sqrt{15\pi}} - l^2 \left( \frac{5\sqrt{5\pi}\bar{\chi}_\rho\bar{G}}{512\bar{\chi}^3\epsilon^3\bar{\phi}\sqrt{12 + \pi}} + \frac{\bar{\chi}\bar{G}\bar{\phi}\sqrt{\pi(12 + \pi)}}{18\sqrt{5}\epsilon^3} \right), \quad (70)$$

where  $\bar{\chi} = \chi(\bar{\phi})$  and  $\bar{\chi}_\rho = (d\chi/d\rho)_{\rho=\bar{\rho}}$ , and we have used the condition that  $\bar{\chi}_\rho \gg (\bar{\chi}/\rho)$  near close packing. Equations (69) and (70) show that the propagating modes are always stable when the density is low or near close packing. The growth rates were calculated for intermediate densities using the Carnahan–Starling approximation for the pair distribution function, and were found to have negative real parts at intermediate density as well.

## 6. Perturbations in the vorticity direction

For perturbations with modulation in the vorticity direction with  $k = 0$  and  $l = 0$ , it is easily verified that  $\Lambda_{\rho x}$ ,  $\Lambda_{\rho y}$ ,  $\Lambda_{x\rho}$ ,  $\Lambda_{xz}$ ,  $\Lambda_{xT}$ ,  $\Lambda_{y\rho}$ ,  $\Lambda_{yz}$ ,  $\Lambda_{yT}$ ,  $\Lambda_{zx}$  and  $\Lambda_{zy}$  in Appendix B are equal to zero. Consequently, the determinant of the dispersion matrix is the product of the determinants of a  $3 \times 3$  matrix, consisting of the density,  $z$ -momentum and energy equation, and a  $2 \times 2$  matrix, which arises from the  $x$ - and  $y$ -momentum equations. The former are referred to as longitudinal modes since they comprise density and momentum variations in the direction of the wave vector, while the latter are called transverse modes since they comprise momentum variations transverse to the direction of the wave vector.

### 6.1. Longitudinal modes

The density and  $z$ -momentum equations give two modes which have growth rates proportional to  $m$  in the limit  $m \rightarrow 0$ ,

$$s_{\rho z} = \pm im \left( \bar{p}_\rho - \bar{G}^2(\bar{\mathcal{C}}_\rho/2 + \bar{\mathcal{F}}_\rho/6) - 2\bar{p} \left( \frac{\epsilon^2 \bar{R}_\rho \bar{T}^{3/2} - \bar{G}^2 \bar{\mu}_\rho}{3\bar{R}\epsilon^2 \bar{T}^{3/2} - \bar{G}^2 \bar{\mu}} \right) \right)^{1/2} - m^2 \left( \frac{\bar{\mu}_b^{**}}{2\bar{\rho}} + \frac{2\bar{\mu}}{3\bar{\rho}} + \frac{\bar{p}^2}{\bar{\rho}(3\bar{R}\epsilon^2 \bar{T}^{3/2} - \bar{G}^2 \bar{\mu})} + \frac{3\bar{\rho} \bar{T} \bar{p} (\bar{R}_\rho \epsilon^2 \bar{T}^{3/2} - \bar{G}^2 \bar{\mu}_\rho)}{(3\bar{R}\epsilon^2 \bar{T}^{3/2} - \bar{G}^2 \bar{\mu})^2} \right), \quad (71)$$

where

$$\bar{\mu}_b^{**} = \bar{\mu}_b + \bar{G}^2(-\bar{\mathcal{H}}/2 + \bar{\mathcal{L}}/2 - \bar{\mathcal{P}}/3 - \bar{\mathcal{Q}}/2 + \bar{\mathcal{T}}/3 + \bar{\mathcal{U}}/6). \quad (72)$$

It is observed that the scaling law for the growth rate as a function of wavenumber is correctly recovered in the Navier–Stokes approximation, and the presence of the Burnett terms results in a quantitative variation in the numerical coefficients. The super-Burnett terms do alter the numerical coefficient of  $m^2$ , but do not affect the scaling of the growth rate with wavenumber.

In the limit of low density, the  $O(m)$  contribution to the growth rate is real,

$$s_{\rho z}^{(l)} = \pm m \bar{G} \left( \frac{\sqrt{5\pi}}{48\epsilon\bar{\phi}} \right) - m^2 \frac{\sqrt{5}\bar{G}\pi}{576\epsilon^3\bar{\phi}^2}, \quad (73)$$

and there is one stable and one unstable mode. There is a stabilizing effect owing to the  $O(m^2)$  term in (71), and this term stabilizes the perturbations for  $m > (12\epsilon^2\bar{\phi}/\sqrt{\pi})$  in the limit of low density. Near close packing, the longitudinal modes are stable and propagating, with equal and opposite imaginary parts proportional to  $m$ ,

$$s_{\rho z}^{(c)} = \pm i \frac{m\bar{G}\bar{\phi}}{\epsilon} \left( \frac{2\bar{\chi}_\rho(12 + \pi)}{15} \right)^{1/2} - m^2 \left( \frac{5\bar{\chi}_\rho\bar{G}}{512\bar{\chi}^3\epsilon^3\bar{\phi}} \left( \frac{5\pi}{12 + \pi} \right)^{1/2} + \frac{\bar{\chi}\bar{G}\bar{\phi}(\pi(12 + \pi))^{1/2}}{18\sqrt{5}\epsilon^3} \right). \quad (74)$$

Thus, there is a transition from unstable to stable modes as the volume fraction is increased.

The stability is determined by the sign of the  $O(m)$  contribution to  $s_{\rho z}$ , which is denoted by  $s'_{\rho z}$ . It is easily verified, by comparing (53) and (71), that  $s'_{\rho z} = (-s_{\rho xy}^3 m^2 / \bar{G} k_0 l_0)^{1/2}$  for  $l_0 \gg \epsilon k_0$ . Therefore, figure 1 also shows the variation of  $(-s_{\rho z}'^2 \epsilon^2 / \bar{G}^2 m^2)$ , and there is a transition from unstable to stable modes when  $(s_{\rho z}'^2 \epsilon / \bar{G}^2 m^2)$  passes through zero in figure 1. The volume fraction for the transition

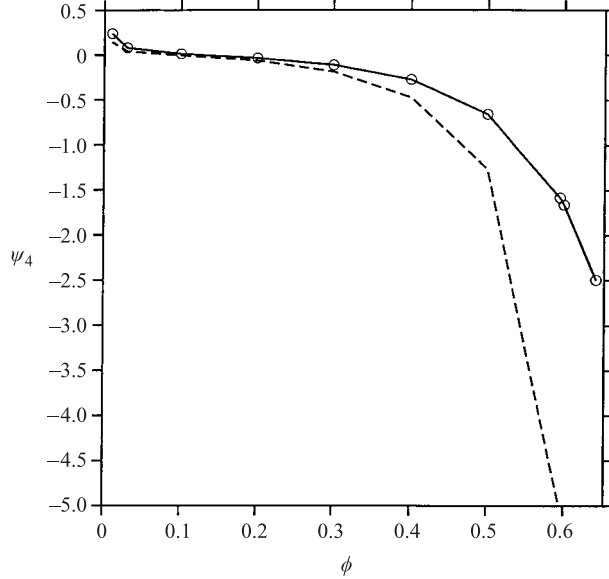


FIGURE 4. Variation of  $\psi_4 = (\bar{\mathcal{A}}/4 - \bar{\mathcal{E}}/2 - \bar{\mathcal{F}}/2)$  with  $\bar{\phi}$ . The solid curve is obtained when the Carnahan–Starling approximation (equation (48)) is used for the pair distribution function, and the broken curve is obtained when the high-density approximation (equation (49)) is used for the pair distribution function.

from unstable to stable modes is  $\phi = 0.149$  in the Carnahan–Starling model, (48), for the pair distribution function and 0.100 in the high-density model, (49).

### 6.2. Transverse modes

The growth rates obtained from the  $x$ - and  $y$ -momentum equations are of the form

$$s_{xy} = \pm m \bar{G} \sqrt{\frac{\bar{\mathcal{A}}}{4\bar{\rho}} - \frac{\bar{\mathcal{E}}}{2\bar{\rho}} - \frac{\bar{\mathcal{F}}}{4\bar{\rho}}} - m^2 \left( \frac{\bar{\mu}}{\bar{\rho}} + \frac{\bar{G}^2}{\bar{\rho}} (\bar{\mathcal{H}}/8 - \bar{\mathcal{P}}/4 - \bar{\mathcal{Q}}/8) \right). \quad (75)$$

In this case, it is observed that there is a qualitative difference in the behaviour of the growth rate in the Navier–Stokes and Burnett approximations, since the Navier–Stokes approximation predicts that these modes are diffusive with the decay rate proportional to  $m^2$ , while the Burnett approximation indicates that the growth rate has a contribution proportional to  $m$  in the long-wave limit. Inclusion of the super-Burnett terms results in a quantitative modification of the coefficient of the term proportional to  $m^2$ .

The stability of these modes depends on the sign of  $(\bar{\mathcal{A}}/4 - \bar{\mathcal{E}}/2 - \bar{\mathcal{F}}/4)$ , which is shown as a function of  $\phi$  in figure 4. In the limit of low density, the solutions for  $s_{xy}$  have the limiting behaviour

$$s_{xy}^{(l)} = \pm m \frac{5}{96} \sqrt{\frac{\pi \bar{G}}{7 \bar{\phi}}} - \frac{\bar{\mu}^{(l)}}{\bar{\rho}} m^2. \quad (76)$$

It is observed that  $(\bar{\mathcal{A}}/4 - \bar{\mathcal{E}}/2 - \bar{\mathcal{F}}/4)$  is positive at low density, so that there are two real solutions for  $s_{xy}$ , one of which is positive in the limit of low wavenumber,



indicating an instability. Near close packing, the limiting behaviour of the solutions of  $s_{xy}$  are

$$s_{xy}^{(c)} = \pm im \frac{\bar{G}(\pi\bar{\phi}_c\bar{\chi})^{1/2}}{2\sqrt{6}} \left( \frac{192}{35\pi} - \frac{4}{35} \right)^{1/2} - \frac{\bar{\mu}^{(c)}}{\bar{\rho}} m^2. \quad (77)$$

Equation (77) indicates that perturbations are stable propagating modes near close packing, in which the growth rate has an imaginary part proportional to  $m$  and real part proportional to  $m^2$ .

At intermediate density,  $(\bar{\mathcal{A}}/4 - \bar{\mathcal{E}}/2 - \bar{\mathcal{F}}/4)$  becomes negative for  $\phi > 0.114$  for the Carnahan–Starling pair distribution function, (48), and for  $\phi > 0.089$  in the high-density approximation, (49), as shown in figure 4. Beyond these densities, the solutions for  $s_{xy}$  are complex conjugates with negative real parts, indicating stable propagating modes. The term proportional to  $m^2$  has a stabilizing effect on the perturbations, and (76) predicts that fluctuations are stabilized for  $m > (48\epsilon\phi/\sqrt{35\pi})$ . The instability at low density, as well as the propagating nature of the fluctuations near close packing, are not captured by the Navier–Stokes model.

## 7. Dilute limit

The growth rates are determined numerically at finite wavenumber for a dilute suspension in the limit of small volume fraction. Since attention is restricted to the short-time limit, where the growth of perturbations are exponential, the wave vectors in this section are denoted by  $(k, l, m)$  without the superscript zero. It is convenient to scale the length and velocity by the mean free path  $(\bar{\rho}d^2)^{-1}$  and  $\bar{T}^{1/2}$ , since these are the relevant length and velocity scales in the dilute limit, and variables scaled in this fashion are denoted by a superscript asterisk. The scaled rate of dissipation of energy, in the base state, is then given by  $4\pi\epsilon^2$ , and the scaled strain rate is  $\bar{G}^* = (64\pi/5)^{1/2}$  from a balance between the rate of production by the mean shear and the dissipation due to inelastic collisions. The growth of perturbations is exponential in the short-time limit, and the results for the scaled growth rate,  $s^*$ , are expressed as a function of the scaled wavenumbers  $k^* = k/(\bar{\rho}d^2)$ ,  $l^* = l/(\bar{\rho}d^2)$  and  $m^* = m/(\bar{\rho}d^2)$ .

Depending on the relative magnitude of the wavenumber and  $\epsilon$ , two regimes can be identified for the growth rate. The rate of dissipation of energy is large compared to the rate of thermal diffusion for  $D_T(k^2 + l^2 + m^2)\bar{T} \ll \bar{\rho}d^2\bar{T}^{3/2}\epsilon^2$ , where the thermal diffusivity  $D_T$  is estimated as  $D_T = \bar{T}^{1/2}/(\bar{\rho}d^2)$ . This is equivalent to  $(k^{*2} + l^{*2} + m^{*2}) \ll \epsilon^2$  in terms of the scaled wavenumber  $k^*$ . The growth rates in this limit evaluated in §4, for perturbations in the flow direction, scaled by  $(\bar{\rho}d^2\bar{T}^{1/2})$ , are

$$\left. \begin{aligned} s_z^* &= \frac{5}{16\sqrt{\pi}} k^{*2}, \\ s_{\rho xy}^{3*} &= -8(\pi/5)^{1/2} \epsilon k^* l^* + 4\sqrt{\pi} \epsilon^2 k^{*2}, \\ s_T^* &= -\frac{8\sqrt{\pi} \epsilon^2}{3}. \end{aligned} \right\} \quad (78)$$

In (78),  $s_T^*$  is the growth rate of energy fluctuations, which tends to a finite value in the limit of small  $\epsilon$ . The growth rates in the limit  $l^* \ll \epsilon$  evaluated in §5, scaled by

( $\bar{\rho}d^2\bar{T}^{1/2}$ ), are

$$\left. \begin{aligned} s_z^* &= \frac{5}{16\sqrt{\pi}}l^{*2}, \\ s_d^* &= -\frac{375l^{*4}}{4096\pi^{3/2}\epsilon^2}, \\ s_p^* &= \pm il^* - \frac{l^{*2}}{8\sqrt{\pi}\epsilon^2}, \\ s_T^* &= -\frac{8\sqrt{\pi}\epsilon^2}{3}. \end{aligned} \right\} \quad (79)$$

The equation for  $s_d^*$  is apparently in contradiction with that for  $s_d^{(l)}$  in (63), since the latter increases proportional to  $l^2$ . However, it should be noted that when  $s_d^{(l)}$  in (63) is expressed in terms of  $l^*$ , the resultant expression is proportional to  $\phi$ , and the coefficient of the term proportional to  $l^{*2}$  approaches zero in the dilute limit. The next non-zero term is the term proportional to  $l^{*4}$ , which is given in (79) for  $s_d^*$ . The growth rates in the limit  $m^* \ll \epsilon$ , evaluated in §6, scaled by ( $\bar{\rho}d^2\bar{T}^{1/2}$ ), are

$$\left. \begin{aligned} s_{\rho z}^* &= \pm im^* - \frac{m^{*2}}{10\sqrt{\pi}\epsilon^2}, \\ s_{xy}^* &= \pm m^* \frac{\pi\epsilon}{2} \sqrt{\frac{5}{7}} - \frac{5}{16\sqrt{\pi}}m^{*2}, \\ s_T^* &= -\frac{8\sqrt{\pi}\epsilon^2}{3}. \end{aligned} \right\} \quad (80)$$

There are three diffusive and two propagating modes for perturbations in the flow and gradient directions, and five diffusive modes for perturbations in the vorticity direction. One of the diffusive modes is unstable in the flow direction, and two of the diffusive modes are unstable in the vorticity direction. All perturbations are stable in the gradient direction.

The rate of dissipation of energy is small compared to the rate of thermal diffusion for  $(k^{*2} + l^{*2} + m^{*2}) \gg \epsilon^2$ . In this case, the dissipation of energy can be neglected in the leading approximation, and the system resembles a gas of elastic particles at equilibrium. The hydrodynamic modes of an elastic gas have been studied in detail, and it is known (Hansen & McDonald 1990) that there are three modes, corresponding to the transverse momentum and energy fluctuations, which are diffusive, and two modes, corresponding to the density and longitudinal momentum, which are propagating. For perturbations in the flow direction, the growth rates are as follows. The transverse ( $y$  and  $z$ ) momentum perturbations have growth rates  $s_y = s_z = -(\mu/\rho)$ . Using  $\mu = (5T^{1/2}/16\sqrt{\pi}d^2)$  in the dilute limit, the scaled growth rates are

$$s_y^* = s_z^* = -\frac{5k^{*2}}{16\sqrt{\pi}}. \quad (81)$$

The growth rate for temperature fluctuations is  $s_T = (-K/\rho C_p)$ , where  $K = (75T^{1/2}/64\sqrt{\pi}d^2)$  in the dilute limit, and the specific heat at constant pressure

$C_p = 5/2$  for a monatomic gas. Using these, the scaled growth rate is

$$s_T^* = -\frac{15k^{*2}}{32\sqrt{\pi}}. \quad (82)$$

The longitudinal modes (density and  $x$  momentum) are propagating with growth rate  $s_{\rho x} = \pm ic_s k - \Gamma k^2$ . Here, the speed of sound  $c_s = (\gamma(\partial p/\partial T)|_\rho)^{1/2}$ , where  $\gamma = 5/3$  is the ratio of specific heats, and the decay rate of the longitudinal modes is  $\Gamma = (1/2)[K(\gamma - 1)/\rho C_p + (4\mu/3 + \mu_b)/\rho]$ . Using  $p = \rho T$ ,  $\mu_b = 0$ ,  $\gamma = 5/3$  and expressions for  $K$ ,  $\mu$  and  $C_p$  provided earlier for the dilute limit, the scaled growth rates of the propagating modes are given by

$$s_{\rho x}^* = \pm ik^* \sqrt{\frac{5}{3}} - \frac{35k^{*2}}{96\sqrt{\pi}}. \quad (83)$$

Since the system is isotropic in this limit, equivalent relations can be obtained for the gradient and vorticity directions. In this case, as well, there are three diffusive and two propagating modes, but all modes are stable.

This transition is analysed using a set of constitutive relations which incorporates the stress tensor correct to Burnett order in the momentum equation, (15), rescaled using  $(\bar{\rho}d^2)^{-1}$  and  $\bar{T}^{1/2}$  as the length and velocity scales, and a modification of the energy equation, (16), which incorporates the heat flux,

$$\rho^* C_v \frac{DT^*}{Dt^*} + p^* G_{ii}^* - 2\mu^* S_{ik}^* S_{ki}^* - \mu_b^* G_{ii}^{*2} + \epsilon^2 R^* T^{*3/2} + \partial_i^* q_i^* = 0, \quad (84)$$

where the heat flux  $q_i$  is given by

$$q_i^* = -\kappa^* \partial_i^* T^* - \kappa'^* \partial_i^* \rho^*. \quad (85)$$

In (85),  $\kappa^*$  is the thermal conductivity which is, in the dilute limit,

$$\kappa^* = \frac{75}{64\sqrt{\pi}}, \quad (86)$$

and the term proportional to  $\kappa'^*$  is the energy flux due to density variations, which is

$$\kappa'^* = \frac{375\epsilon^2}{128\sqrt{\pi}} \quad (87)$$

in the dilute limit (Sela & Goldhirsch 1998). Since  $\kappa'$  is proportional to  $\epsilon^2$ , the contribution to the heat flux due to density variations turns out to be numerically small. Numerical calculations show that this contribution is about 5% of the energy flux due to temperature variations even at  $\epsilon = 0.5$ . However, this contribution is retained in the results reported below.

The growth rates of the hydrodynamic modes are obtained using the momentum conservation equation incorporating the stress tensor in (15), and the energy conservation equation, (84), using the heat flux in (85). It is expected that as the wavenumber is increased from values smaller than  $\epsilon$  to values larger than  $\epsilon$ , the growth rates undergo a transition from the scaling laws in (78), (79) and (80) to the scaling laws in (81), (82) and (83), and the unstable modes in the limit  $(k^*, l^*, m^*) \ll \epsilon$  become stable for  $(k^*, l^*, m^*) \gg \epsilon$ . This transition is shown as a function of wavenumber for  $\epsilon = 0.01$  for perturbations in the flow, gradient and vorticity directions in figures 5, 6, 7 and 8, and for  $\epsilon = 0.1$  in figures 9, 10, 11 and 12. In the flow direction (figures 5 and 9), there are three diffusive and two propagating modes in the limits  $k^* \ll \epsilon$  and  $k^* \gg \epsilon$ , but the scalings of the growth rate with wavenumber are very different in the

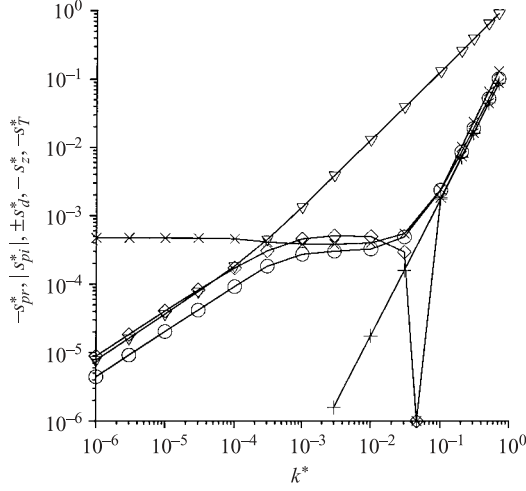


FIGURE 5. The growth rates  $-s_{pr}^*$  ( $\circ$ ),  $|s_{pi}^*|$  ( $\nabla$ ),  $s_d^*$  ( $\diamond$ ),  $-s_d^*$  ( $*$ ),  $-s_z^*$  ( $+$ ),  $-s_T^*$  ( $\times$ ) as a function of  $k^*$  at  $\epsilon = 0.01$ ,  $l^* = 0$ ,  $l^* = 0$ .

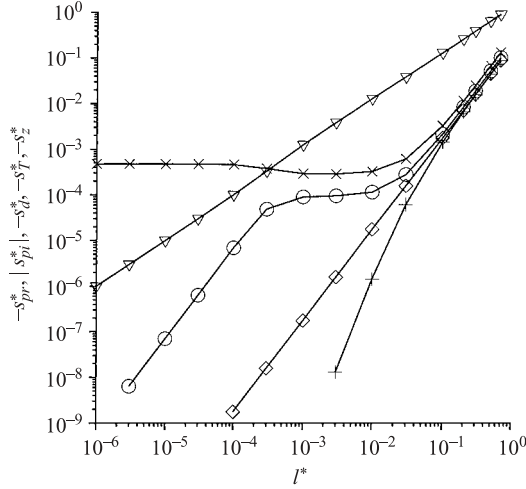


FIGURE 6. The growth rates  $-s_{pr}^*$  ( $\circ$ ),  $|s_{pi}^*|$  ( $\nabla$ ),  $-s_z^*$  ( $\diamond$ ),  $-s_d^*$  ( $+$ ),  $-s_T^*$  ( $\times$ ) as a function of  $l^*$  at  $\epsilon = 0.01$ ,  $k^* = 0$ ,  $m^* = 0$ .

two limits. The growth rate of the temperature mode,  $s_T^*$ , is negative and approaches a constant value in the limit  $k^* \ll \epsilon$ , while its magnitude increases proportional to  $k^{*2}$  for  $k^* \gg \epsilon$ . The unstable diffusive solution for  $s_{\rho_{xy}}$  in (78) (denoted by  $s_d^*$  in figure 5) increases proportional to  $k^{*2/3}$  for  $k^* \ll \epsilon$ , but decreases and becomes negative for  $k^* \sim \epsilon$ . The magnitude of the growth rate of this mode converges to the value for the transverse momentum mode (81) in the limit  $k^* \gg \epsilon$ . The growth rate of the other transverse momentum mode,  $s_z^*$ , increases proportional to  $k^{*2}$  in the limits  $k^* \ll \epsilon$  and  $k^* \gg \epsilon$ . The magnitudes of the real and imaginary parts of the propagating mode increase proportional to  $k^{*2/3}$  for  $k^* \ll 1$ , and exhibit the scaling given in (83) for  $k^* \gg 1$ . Perturbations in the gradient direction show a transition from the scaling behaviour in (79) for  $l^* \ll \epsilon$  to the scalings in (81), (82) and (83) for  $l^* \gg \epsilon$ , as shown in figures 6 and 10. The magnitude of the growth rate of the diffusive mode

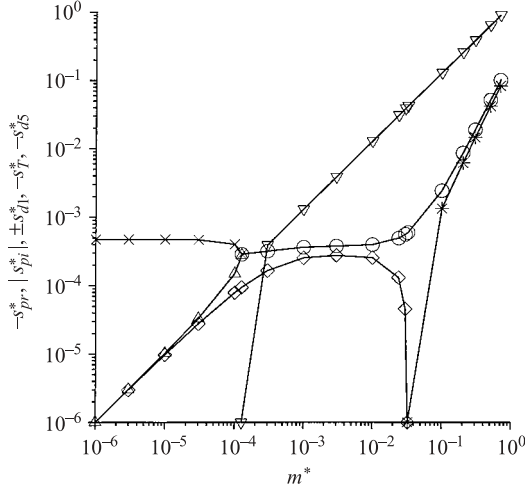


FIGURE 7. The growth rates  $-s_{pr}^*$  ( $\circ$ ),  $|s_{pi}^*|$  ( $\nabla$ ),  $s_{d1}^*$  ( $\diamond$ ),  $-s_{d1}^*$  ( $*$ ),  $-s_{d5}^*$  ( $\triangle$ ),  $-s_T^*$  ( $\times$ ) as a function of  $m^*$  at  $\epsilon = 0.01$ ,  $k^* = 0$ ,  $l^* = 0$ .

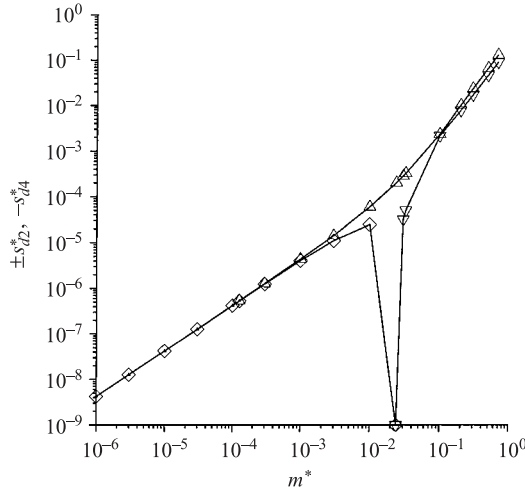


FIGURE 8. The growth rates  $s_{d2}^*$  ( $\diamond$ ),  $-s_{d2}^*$  ( $\nabla$ ),  $s_{d4}^*$  ( $\triangle$ ) as a function of  $m^*$  at  $\epsilon = 0.01$ ,  $k^* = 0$ ,  $l^* = 0$ .

$s_d^*$  increases proportional to  $l^{*4}$  for  $l^* \ll \epsilon$ , and proportional to  $l^{*2}$  for  $l^* \gg \epsilon$ . In the vorticity direction, the situation is more complicated, as shown in figures 7 and 8 for  $\epsilon = 0.01$ , and in figures 11 and 12 for  $\epsilon = 0.1$ . There are five diffusive modes in the limit  $m^* \ll \epsilon$ , which are labelled  $s_{d1}^*$  to  $s_{d5}^*$ . Of these,  $s_{d3}^*$  corresponds to the growth rate of damped energy perturbations in the limit  $m^* \ll \epsilon$ ;  $s_{d1}^*$  and  $s_{d2}^*$  are the growth rates of the unstable modes for  $m^* \ll \epsilon$ , and  $s_{d4}^*$  and  $s_{d5}^*$  are the growth rates of the stable modes in this limit. As  $m^*$  is increased, there is transition from five diffusive modes to two propagating and three diffusive modes at the wavenumber  $m_{d \rightarrow p}^*$  owing to the coalescence of two of the diffusive modes, one of which corresponds to thermal diffusion in the low  $m^*$  limit. Figures 5–8 show that there are two distinct regimes, one of which shows the scaling behaviour when energy conduction is neglected in comparison to dissipation for  $(k^*, l^*, m^*) \ll 1$ , and a second scaling behaviour when

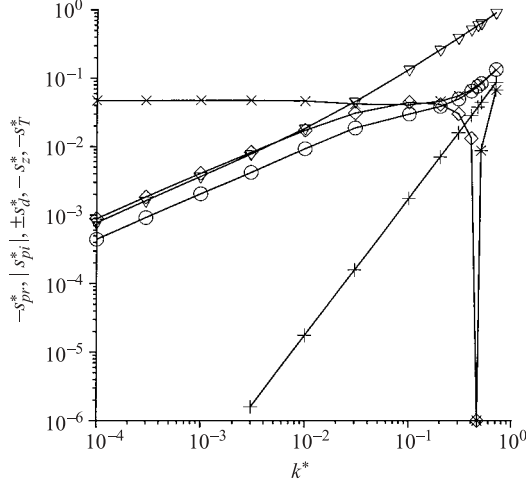


FIGURE 9. The growth rates  $-s_{pr}^*$  ( $\circ$ ),  $|s_{pi}^*|$  ( $\nabla$ ),  $s_d^*$  ( $\diamond$ ),  $-s_d^*$  ( $*$ ),  $-s_z^*$  ( $+$ ),  $-s_T^*$  ( $\times$ ) as a function of  $k^*$  at  $\epsilon = 0.1$ ,  $l^* = 0$ ,  $m^* = 0$ .

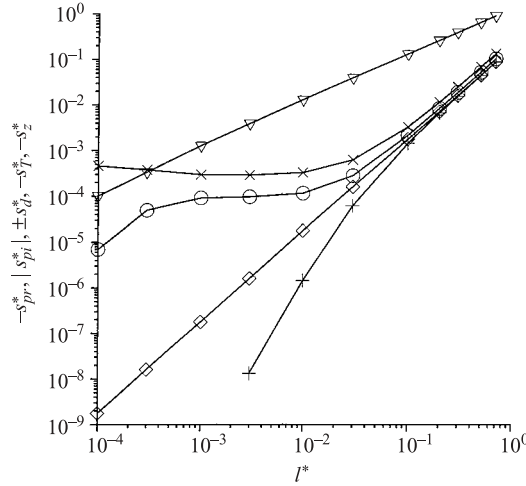


FIGURE 10. The growth rates  $-s_{pr}^*$  ( $\circ$ ),  $|s_{pi}^*|$  ( $\nabla$ ),  $-s_z^*$  ( $\diamond$ ),  $-s_d^*$  ( $+$ ),  $-s_T^*$  ( $\times$ ) as a function of  $l^*$  at  $\epsilon = 0.1$ ,  $k^* = 0$ ,  $m^* = 0$ .

energy conduction is dominant for  $(k^*, l^*, m^*) \gg \epsilon$ . This distinction is not as clear for  $\epsilon = 0.1$  (figures 9–12), because the scaling in (78), (79) and (80) persists over a larger range of wavenumber, and the scaling in (81), (82) and (83) is not as easily discernible, since the range  $k^* > \epsilon$  spans less than a decade.

The wavenumber for transition from unstable to stable perturbations in the flow direction  $k_t^*$ , and the wavenumbers  $m_{t1}^*$  and  $m_{t2}^*$  for the transition of the two diffusive modes in the vorticity direction, increase proportional to  $\epsilon$ , as shown in figure 13. The wavenumber for transition from five diffusive to three diffusive and two propagating modes in the vorticity direction,  $m_{d \rightarrow p}^*$ , increases proportional to  $\epsilon^2$  in the low  $\epsilon$  limit.

As indicated earlier, perturbations are unstable when the wavenumber is small compared to  $\epsilon$  and energy conduction is neglected, but they become stable when the wavenumber is large compared to  $\epsilon$ . Because of this, it is expected that the

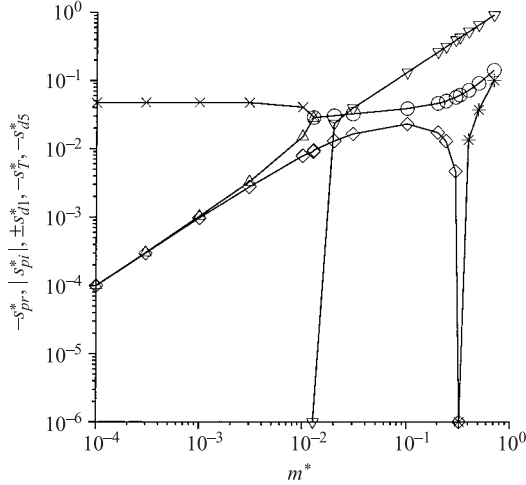


FIGURE 11. The growth rates  $-s_{pr}^*$  (○),  $|s_{pi}^*|$  (▽),  $s_{d1}^*$  (◇),  $-s_{d1}^*$  (\*),  $-s_{d5}^*$  (△),  $-s_T^*$  (×) as a function of  $m^*$  at  $\epsilon = 0.1$ ,  $k^* = 0$ ,  $l^* = 0$ .

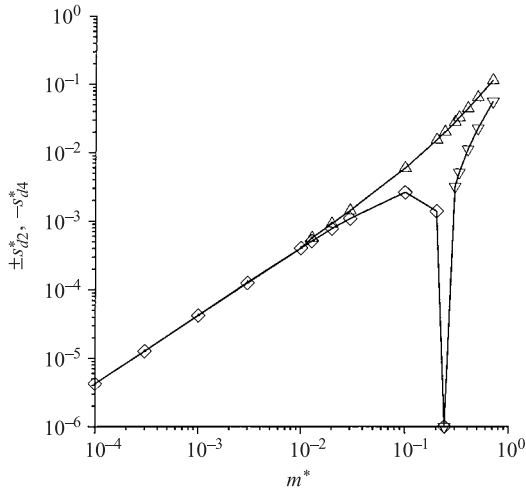


FIGURE 12. The growth rates  $s_{d2}$  (◇),  $-s_{d2}$  (▽),  $s_{d4}$  (△) as a function of  $m^*$  at  $\epsilon = 0.1$ ,  $k^* = 0$ ,  $l^* = 0$ .

wavenumber for transition from unstable to stable modes will be proportional to  $\epsilon$  in the small  $\epsilon$  limit. The instability in the low-wavenumber limit is a transient instability in the flow direction, since the flow rotates the perturbations to align with the gradient direction at long times. However, the instability is an absolute instability in the gradient and vorticity directions. The neutral stability curves in the gradient-vorticity plane are shown in figure 14. It is more convenient to plot  $(l^*/\epsilon)$  versus  $(m^*/\epsilon)$ , since the transition wavenumbers decrease proportional to  $\epsilon$  in the small  $\epsilon$  limit. Figure 14 shows that the neutral stability curves collapse onto the  $\epsilon \rightarrow 0$  limiting curve for  $\epsilon \leq 0.3$ , but there is some variation in the neutral stability curves for  $\epsilon = 0.5$  and  $\epsilon = 0.7$ . Since perturbations are unstable at low wavenumber in the vorticity direction, the neutral stability curves converge to finite value of  $(m^*/\epsilon)$  in the limit  $(l^*/\epsilon) \rightarrow 0$ .

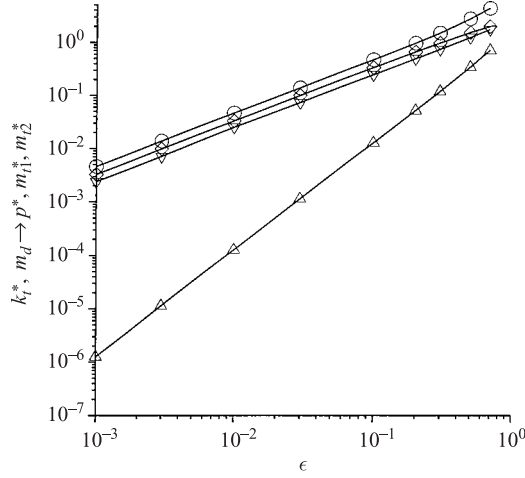


FIGURE 13. The wavenumber for transition from unstable to stable perturbations in the flow direction  $k_t^*$  ( $\circ$ ), the wavenumber for transition from five diffusive to three diffusive and two propagating modes in the vorticity direction  $m_{d \rightarrow p}^*$  ( $\triangle$ ), the wavenumbers  $m_{t1}^*$  ( $\nabla$ ) and  $m_{t2}^*$  ( $\diamond$ ) above which the two diffusive modes in the vorticity direction become stable, as a function of  $\epsilon$ .

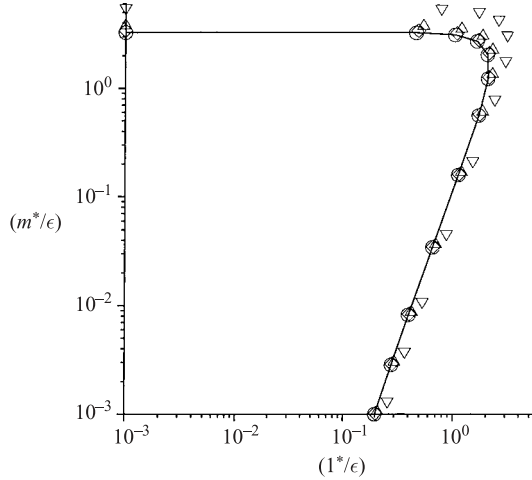


FIGURE 14. Neutral stability curves in the  $(l^*/\epsilon), (m^*/\epsilon)$ -plane for  $\epsilon = 0.1$  ( $\circ$ ),  $\epsilon = 0.3$  ( $\diamond$ ) and  $\epsilon = 0.5$  ( $\triangle$ ),  $\epsilon = 0.7$  ( $\nabla$ ), and in the limit  $\epsilon \rightarrow 0$  (solid line).

The analysis of § 5 has shown that perturbations are stable in the gradient direction in the dilute limit, and so it is expected that the transition wavenumber in the gradient direction should tend to zero for  $(m^*/\epsilon) \rightarrow 0$ . Figure 14 indicates that  $(l^*/\epsilon) \propto (m^*/\epsilon)^{1/3}$  in this limit, confirming that the results of this section are in agreement with those of § 5 in the dilute limit.

## 8. Conclusions

The constitutive relation for the granular flow of smooth, inelastic, spherical particles was derived in § 2 in the adiabatic limit where the length scale for the conduction of energy is small compared to the macroscopic scale. In this case, the



temperature is not a conserved variable, and the rate of change of temperature is determined by a balance between the source and dissipation of energy. The velocity distribution function was assumed to be a Gaussian distribution in which the temperature  $T_{ij}$ , which is the mean square of the fluctuating velocity  $\langle c_i c_j \rangle$ , is not isotropic. This is inserted into the balance equation for the second moment of the velocity distribution, and solved using an asymptotic expansion in the parameter  $\epsilon = (1 - e)^{1/2}$ . The stress tensor was then calculated from the distribution function, and inserted into the momentum equations to obtain equations for the velocity field. Since energy is a non-conserved variable, the stress tensor does not contain terms that depend on the gradients of the temperature (apart from those obtained from the dependence of the viscometric coefficients on the temperature).

The terms in the stress tensor were calculated correct to  $O(\epsilon^2)$ . The leading-order terms correspond to those obtained in the Euler approximation, in which the pressure is isotropic, and the  $O(\epsilon)$  terms correspond to those in the Navier–Stokes approximation where the viscous stress appears. The  $O(\epsilon^2)$  terms correspond to the Burnett approximation, which contain normal stress differences. It should be noted that in the classical kinetic theory, these correspond to terms that are proportional to the zeroth, first and second powers of the rate of deformation tensor. However, in the present case, all terms are quadratic functions of the rate of deformation tensor, owing to the dependence of the temperature on the rate of deformation tensor. It is found that the terms obtained in the present calculation in the Navier–Stokes approximation are accurate to within 1.2% of the analogous terms in the Chapman–Enskog theory dense gases, and are in exact agreement with a simplified Chapman–Enskog result when the Sonine polynomial expansion for the distribution function is truncated at the first term. The terms in the Burnett approximation are accurate to within 6.5% of the Chapman–Enskog theory for dilute gases, and are in exact agreement with a simplified Chapman–Enskog result when the Sonine polynomial expansion is truncated at the first term. Thus, the results for the second-order closure scheme, when energy is treated as a non-conserved variable, are in agreement with the results of the Enskog procedure when energy is treated as a conserved variable where the temperature is determined by the energy balance equation. The close agreement in the numerical values of the coefficients indicates that the anisotropic Gaussian captures the perturbed distribution function accurately. The advantage of this procedure is that the calculation is simpler than the Chapman–Enskog expansion, and the Burnett approximation is obtained for dense gases as well. The constitutive relation in the Navier–Stokes approximation is also of the same form as those of Jenkins & Savage (1983) and Lun *et al.* (1984), and the terms up to Burnett order are identical to those of Sela & Goldhirsch (1998), if the Burnett terms in the stress tensor proportional to the temperature gradients are neglected. However, Sela & Goldhirsch also calculate the  $O(\epsilon^2)$  correction to the viscosity, which is  $O(\epsilon)$  smaller than the smallest terms retained here. The formulation can be systematically extended to determine the super-Burnett terms, though this was not carried out owing to algebraic complexity. However, the super-Burnett terms, which are cubic functions of the rate of deformation tensor, were incorporated in the linear stability analysis, and the effect of these terms on the decay of the hydrodynamic modes was examined even though the coefficients in these terms were not explicitly calculated. The simplification in the present procedure is that it is not necessary to specify boundary conditions for the temperature or the heat flux. There will be a modification to the temperature near the boundaries owing to the nature of the boundary surfaces, but these are restricted to distances of the order of the conduction length from the boundary.

Even though the results obtained here are similar to those obtained in the usual Chapman–Enskog procedure, it is important to note that the procedure used is qualitatively different. In a gas at equilibrium, Newton’s law for viscosity provides terms that are proportional to the gradient of the mean velocity, while the Burnett terms are proportional to the second spatial derivative of the velocity and quadratic functions of the velocity gradient. Therefore, the stresses in the Navier–Stokes approximation is a linear function of the wavenumber, while the stress in the Burnett approximation is a quadratic function of the wavenumber. In a driven system, however, the stresses in the Navier–Stokes and Burnett approximations contain linear functions of the wavenumber because there is a mean velocity gradient. Therefore, the Euler, Navier–Stokes and Burnett terms are obtained using an expansion in  $\epsilon$  in the present analysis, in contrast to the expansion in gradients in the usual Chapman–Enskog procedure, and the Navier–Stokes and Burnett terms contribute at equal order in the wavenumber expansion in a sheared granular material. In this situation, it is of interest to determine whether inclusion of terms that are higher order in  $\epsilon$  results in qualitative variations in the structure of the hydrodynamic modes, or whether the variation is only quantitative so that a Navier–Stokes description with renormalized pressure and viscosity is adequate. This issue was examined in §§4, 5 and 6.

The constitutive relation evaluated in §2 was used to determine the decay rates of the hydrodynamic modes for a linear shear flow in §§4, 5 and 6. Since a constant velocity gradient is imposed on the material, it is not possible to obtain an eigenvalue problem using wave vectors that are independent of time, and it is necessary to analyse the flow using time-dependent wave vectors which turn with the flow. Because of this, the dispersion matrix is a function of time for perturbations with modulation in the flow direction, while it is time-independent for perturbations with modulation in the gradient and vorticity directions. Both the short-time and long-time asymptotic behaviour of the hydrodynamic modes were analysed for perturbations with modulation in the flow direction.

For perturbations with modulation in the plane of flow, there is a decoupling between the  $z$ -momentum equation and the other three conservation equations. The mode corresponding to  $z$ -momentum variations shows typical diffusive behaviour, with decay rate proportional to  $(k^2 + l^2)$ . The decay rate of the other three modes are qualitatively different. In the small-time limit, the growth rates are proportional to  $(-1)^{1/3} \bar{G} k_0^{2/3}$  for  $\bar{G} \bar{\mu}_\rho k_0 \gg \bar{p}_\rho l_0$ , and  $-(-1)^{1/3} \bar{G} k_0^{1/3} l_0^{1/3}$  for  $\bar{G} \bar{\mu}_\rho k_0 \ll \bar{p}_\rho l_0$ , where  $k_0$  and  $l_0$  are the wavenumbers at zero time. This unusual 2/3 power law scaling of the growth rate with wave vector is due to the coupling between the  $x$ - and  $y$ -momentum equations due to the density dependences of the pressure and viscosity. In addition, it is observed that there are one or two growing modes at early-times at all densities, except at a particular density of when all modes are neutrally stable and there is an exchange of stability. The early-time results also indicate that the qualitative behaviour of the growth of perturbations is accurately captured by the Navier–Stokes model.

In the long-time limit, the growth rate of perturbations in the plane of flow depends on the constitutive model used. In the Navier–Stokes approximation, the slowest decaying modes have a decay rate proportional to  $k_0^2 \bar{G}^3 t^2$ , resulting in a 2/3 power-law dependence of the decay rate on the wavenumber owing to the turning of the wave vector by the mean flow. Though the analysis was not carried out for the Burnett and super-Burnett approximations, it was anticipated that the growth rate in these cases scale as  $k_0^3 \bar{G}^4 t^3$  and  $k_0^4 \bar{G}^5 t^4$  respectively. Thus, it appears that the long-time behaviour is sensitive to the constitutive model for the stress, and it is necessary to

carry out the analysis with higher-order terms in the constitutive equation for the stress tensor to ascertain whether perturbations do decay in the long-time limit for  $k_0 \bar{G}t \sim 1$ . However, it should be noted that there is an upper bound on the  $t$  for which the analysis is valid. This is because a low wavenumber analysis has been used, and it is implicitly assumed that the scaled wavenumber is small compared to 1. As time progresses, the wavenumber in the gradient direction increases as  $l = l_0 + \bar{G}k_0 t$ , and the scaled wavenumber  $l$  is not small for  $t \sim (\bar{G}k_0)^{-1}$ , even though the initial wavenumber in the flow direction  $k_0$  may be small. In this case, a hydrodynamic analysis breaks down, since the length scale is smaller than the microscopic scale. It can only be concluded that if the perturbations decay at long times in this regime, the maximum amplitude of fluctuations, as well as the initial growth and subsequent decay, can be adequately described by the Navier–Stokes approximation.

For perturbations with modulation in the gradient direction, there are two propagating modes in which the growth rates are complex conjugates with imaginary parts proportional to  $l$  and real parts proportional to  $l^2$ , and one diffusive mode in which the growth rate has a real part proportional to  $l^2$ . The propagating modes are stable, and the dependence of the growth rate on the wavenumber is captured by the Navier–Stokes model, though there are quantitative corrections due to the Burnett terms. The diffusive mode is stable at low density, but becomes unstable when the volume fraction exceeds 0.154 to 0.217 depending on the model for the pair distribution function. The present calculation predicts that this mode is unstable in the limit of high density, and is the most unstable mode in this limit. The Burnett and super-Burnett corrections do not affect the stability characteristics of this mode. In order to determine the range of wavenumbers for which the diffusive mode is unstable, it was necessary to calculate the next correction to the growth rate in the wavenumber expansion, which turned out to be proportional to  $l^4$ . It was found that this contribution is stabilizing, and the conduction of energy has a significant effect on this contribution. In the limit of high density, the range of wavenumbers for instability decreased proportional to  $\chi(\phi)^{-1/2}$  where  $\chi$  is the pair distribution function which diverges at close packing. In addition, the maximum growth rate of perturbations remains finite and numerically small at all densities. The combination of a low growth rate and a small range of unstable wavenumbers would make this instability difficult to detect, especially for studies carried out on finite-size systems.

For perturbations with modulation in the vorticity direction, there is a decoupling of the dispersion matrix into a  $3 \times 3$  matrix, which couples the fluctuations in the density,  $z$ -momentum and temperature (longitudinal modes), and a  $2 \times 2$  matrix which couples the  $x$ - and  $y$ -momenta (transverse modes). In the limit of small wave vector, the growth rate for the longitudinal modes has a real and negative part proportional to  $m^2$ , and contributions equal in magnitude and opposite in sign proportional to  $m$ . The contributions proportional to  $m$  are real in the limit of low density, indicating that there is one stable and one unstable mode. In the limit of high density, the contributions proportional to  $m$  are imaginary, indicating the presence of two stable propagating modes. There is a transition from unstable to stable modes at a volume fraction between 0.1 and 0.149 depending on the model for the pair distribution function. It is found that the Burnett and super-Burnett corrections do not alter the qualitative behaviour of these modes. The growth rates for the  $x$ - and  $y$ -momentum perturbations, in the leading approximation, are given by  $s_{xy} = \pm m \bar{G} \bar{\rho} (\bar{\mathcal{A}}/4 - \bar{\mathcal{E}}/2 - \bar{\mathcal{F}}/4)^{1/2} - m^2 (\bar{\mu}/\bar{\rho})$ . In this case, it is found that the Burnett corrections affect the qualitative nature of these modes, since the component of the growth rate proportional to  $m$  is not captured by the Navier–Stokes

approximation. However, the super-Burnett corrections do not qualitatively change the nature of these modes. In the limit of low-density, there are two real solutions for the growth rate proportional to  $m$ , one of which is positive and the other negative, indicating that these modes are unstable in the low-density limit. In the limit of high density, the contribution proportional to  $m$  is imaginary, and the transverse modes are damped propagating modes. In the intermediate density regime, there is a transition from unstable to stable modes when the density is increased beyond 0.089 – 0.114 depending on the model used for the pair distribution function.

When the wavelength of perturbations is small compared to the conduction length, the conduction of energy is large compared to dissipation, and the structure of the hydrodynamic modes is expected to be identical to that for a gas of elastic particles. In this case, there are three diffusive modes (corresponding to transverse momentum and energy perturbations) and two propagating modes (corresponding to density and longitudinal momentum perturbations). All modes are stable in this limit. As the wavenumber undergoes a transition from  $(k, l, m) \ll \epsilon$  to  $(k, l, m) \gg \epsilon$ , there is expected to be a transition from the scaling derived in §§4, 5 and 6 to that for a system of elastic particles. This transition was analysed in §7 for a granular flow in the dilute limit, where the Burnett approximation for the stress tensor was used in the momentum balance equations, and the energy balance equation incorporated the divergence of the heat flux due to temperature and density gradients. This generalized hydrodynamic model showed the transition from the growth rates in §§4, 5 and 6 to the growth rates for a system of elastic particles for  $\epsilon = 0.01$ , though the transition was less clear for  $\epsilon = 0.1$ , since the range of wavenumbers was not sufficient to infer scaling laws. This result provides further verification that energy conduction can be neglected at length scales large compared to the conduction length.

In the dilute limit, it was verified that the scaling of the growth rate with wavenumber and with  $\epsilon$  are in agreement with the scaling obtained (Kumaran 2001*a, b*) using a more detailed description where the higher moments of the velocity distribution are included. Thus, the present description, which includes the Burnett terms, is adequate for describing the stability of a sheared granular flow in the long-wave limit. The Navier–Stokes description is not adequate for this purpose, since the predictions for the growth rate in the vorticity direction depend on the Burnett-order terms. The stability analysis is also in agreement with the initial time studies of Savage (1992) and Babic (1993), which indicated the presence of unstable modes in all three directions at short time. The results for perturbations in the plane of flow at long time are in agreement with the results of Schmid and Kytomaa for the momentum fluctuations. However, since Schmid & Kytomaa (1994) included the conduction term for the temperature, they obtained an additional term in the temperature equation which decays as  $\exp(-(\kappa/\bar{\rho}C_v)k_0^2 t^3/3)$ , where  $\kappa$  is the thermal conductivity. The present analysis indicates that the diffusive mode in the gradient direction becomes unstable when the volume fraction exceeds a minimum value, but the growth rate of this is numerically small, and there is a stabilizing effect which is higher order in wavenumber. This is in agreement with the analysis of Babic (1993), which also predicts an instability in the gradient direction in the low-wavenumber regime, though the dependence of the growth rate on the wavenumber and density was not systematically analysed. This turns out to be the most unstable mode at high-volume fraction. At low-volume fraction, the present analysis predicts that there are two unstable modes in the vorticity direction. One of these is not captured by the earlier studies which use modified Navier–Stokes approximations, since the growth rate is proportional to the coefficients in the Burnett-order contributions to the stress tensor.

Though the results of the present analysis are qualitatively similar to those of Savage (1992), Babic (1993) and Schmid & Kytomaa (1994), the present study uses an expansion in the wavenumber to obtain analytical results for the growth rate of the perturbations. In this manner, two distinct regimes are identified, one where the length scale is large compared to the conduction length (wavelength small compared to  $\epsilon$ ), and the other where the length scale is small compared to the conduction length (wavelength large compared to  $\epsilon$ ). In the former, the rate of conduction is small compared to the rate of dissipation, and energy is treated as an active scalar which is determined by the balance between the rate of production due to shear flow and the rate of dissipation due to inelastic collisions. Perturbations are found to be unstable in this regime in the vorticity direction at small-volume fraction, and in the gradient direction at higher-volume fraction. It is also found that the Burnett approximation for the stress tensor is necessary for accurately capturing the growth rates of the hydrodynamic modes. In the opposite limit, the rate of conduction is large compared to the rate of dissipation, and energy is treated as a conserved variable in the leading approximation. The hydrodynamic modes in this case are identical to those for a gas of elastic particles at equilibrium, and there are two propagating and three diffusive modes, all of which are stable. The identification of these regimes, and the scaling of the transition wavenumber with  $\epsilon$  for the transition from unstable to stable modes, has not been systematically analysed earlier. The present study also reveals that a uniform approximation for the equations of motion, which incorporates the strain-rate-dependent Burnett terms in the stress equation (neglecting the temperature-dependent Burnett terms), and the Fourier law for heat conduction in the energy equation (neglecting all the Burnett terms), is the minimal model which captures the dynamics of the flow in both regimes.

The results of § 7 provide the neutral stability curves in the gradient–vorticity plane as a function of the parameter  $\epsilon$ . These results can be tested by simulations, in which the smallest allowable wavenumber in the gradient and vorticity directions can be varied by varying the system size, in order to examine the stability of the perturbations. In addition, the analysis in §§ 5 and 6 provides numerical results for the volume fraction for the transition from stable to unstable perturbations in the gradient and vorticity directions for two specific forms of the pair distribution function. Though the actual volume fraction for transition is dependent on the form of the pair distribution function, the qualitative nature of the transition from stable to unstable perturbations could be examined in simulations. A more rigorous test of the analysis would be to examine the growth or decay of time-displaced correlation functions in the gradient and vorticity directions using techniques used for deriving transport coefficients from correlation functions in molecular dynamics simulations (Allen & Tildesley 1990).

## Appendix A

The collision integral for the second moment, correct to  $O(\epsilon^2 T)$ , using the procedure given in § 2, is

$$\begin{aligned} \frac{\partial_c(\rho \langle c_i c_j \rangle)}{\partial t} = \frac{6\rho\phi\chi(\phi)}{\pi} & \left[ -\epsilon\sqrt{\pi}\frac{16T_{ij}^{(1)}T^{1/2}}{5} - \epsilon^2\sqrt{\pi}\left(\frac{8T^{3/2}\delta_{ij}}{3} \right. \right. \\ & \left. \left. + \frac{16T_{ij}^{(2)}T^{1/2}}{5} + \frac{16(T_{ik}^{(1)}T_{kj}^{(1)} - (\delta_{ij}/3)T_{kl}^{(1)}T_{lk}^{(1)})}{35T^{1/2}} \right) \right] \end{aligned}$$

$$\begin{aligned}
& -\frac{4\pi T}{15} \left( 2S_{ij} + \frac{5}{3}\delta_{ij}G_{kk} \right) \\
& + \frac{16\sqrt{\pi}T^{1/2}}{105} \left( \frac{14}{3}S_{ij}G_{kk} + 4S_{ik}S_{kj} + \delta_{ij}S_{kl}S_{lk} + \frac{35}{18}\delta_{ij}G_{kk}^2 \right) \\
& + \frac{8\pi\epsilon}{105} \left( \frac{14}{3}T_{ij}^{(1)}G_{kk} + T_{ik}^{(1)}S_{kj} + T_{jk}^{(1)}S_{ki} - 3\delta_{ij}T_{kl}^{(1)}S_{lk} \right) \Bigg], \quad (\text{A } 1)
\end{aligned}$$

where the volume fraction  $\phi$  is  $(\pi\rho/6)$ .

This can be inserted into the second moment equation (6) and solved systematically to obtain the matrix  $T_{ij}$  in terms of the strain rate tensor  $G_{ij}$ .

$$\rho \frac{DT_{ij}}{Dt} + \rho(T_{ik}G_{kj} + T_{jk}G_{ki}) = \frac{\partial_c \rho \langle c_i c_j \rangle}{\partial t}. \quad (\text{A } 2)$$

The solution for  $T_{ij}^{(1)}$  is obtained from the  $O(\epsilon)$  contribution to the symmetric traceless part of the second moment equation,

$$\rho T(G_{ij} + G_{ji} - 1/3\delta_{ij}G_{kk}) = \left( \frac{\partial_c}{\partial t} (\rho \langle c_i c_j - 1/3c^2 \delta_{ij} \rangle) \right) \Bigg|_1, \quad (\text{A } 3)$$

where  $(\cdot)|_1$  denotes the  $O(\epsilon)$  contribution to  $(\cdot)$ . This is easily solved to obtain

$$\epsilon T_{ij}^{(1)} = -S_{ij}T^{1/2}Q(\phi), \quad (\text{A } 4)$$

where  $S_{ij} = (G_{ij} + G_{ji} - (2\delta_{ij}/3)G_{kk})/2$  is the symmetric traceless part of the rate of deformation tensor, and

$$Q(\phi) = \frac{5\sqrt{\pi}}{48\phi\chi(\phi)} \left( 1 + \frac{8\phi\chi(\phi)}{5} \right). \quad (\text{A } 5)$$

The second correction  $T_{ij}^{(2)}$  is determined in a similar fashion from the second correction to (A 2),

$$-\rho \frac{D(T^{1/2}S_{ij}Q(\phi))}{Dt} - \rho T^{1/2}Q(\phi)(G_{ik}S_{kj} + G_{jk}S_{ki}) = \left( \frac{\partial_c}{\partial t} (\rho \langle c_i c_j - 1/3c^2 \delta_{ij} \rangle) \right) \Bigg|_2, \quad (\text{A } 6)$$

where  $(\cdot)|_2$  denotes the  $O(\epsilon^2)$  contribution to  $(\cdot)$ . The substantial derivative on the left-hand side of (A 6) is simplified as

$$\frac{D(T^{1/2}S_{ij}Q(\phi))}{Dt} = S_{ij}T^{1/2} \frac{dQ}{d\rho} \frac{D\rho}{Dt} + \frac{S_{ij}Q(\phi)}{2T^{1/2}} \frac{DT}{Dt} + T^{1/2}Q(\phi) \frac{DS_{ij}}{Dt} \quad (\text{A } 7)$$

$$= -S_{ij}T^{1/2} \frac{dQ}{d\rho} \rho G_{ii} + \frac{S_{ij}Q(\phi)}{2T^{1/2}} \frac{DT}{Dt} + T^{1/2}Q(\phi) \frac{DS_{ij}}{Dt}, \quad (\text{A } 8)$$

where the substitution  $(D\rho/Dt) = -\rho G_{ii}$  (mass conservation) has been used. The terms on the right-hand side of (A 8) are evaluated as follows. The substantial derivative of the symmetric part of the rate of deformation tensor is

$$\begin{aligned}
\frac{DS_{ij}}{Dt} &= \left( \frac{\partial S_{ij}}{\partial t} + u_k \frac{\partial S_{ij}}{\partial x_k} \right) \\
&= \frac{1}{2} \left( \frac{\partial}{\partial x_i} \frac{Du_j}{Dt} + \frac{\partial}{\partial x_j} \frac{Du_i}{Dt} - \frac{2\delta_{ij}}{3} \frac{\partial}{\partial x_k} \frac{Du_k}{Dt} - G_{ik}G_{kj} - G_{jk}G_{ki} + \frac{2\delta_{ij}}{3} G_{kl}G_{lk} \right)
\end{aligned}$$

$$\begin{aligned}
&= \frac{1}{2} \left( \frac{\partial}{\partial x_i} \left( \frac{1}{\rho} \frac{\partial \sigma_{jk}}{\partial x_k} \right) + \frac{\partial}{\partial x_j} \left( \frac{1}{\rho} \frac{\partial \sigma_{ik}}{\partial x_k} \right) - \frac{2\delta_{ij}}{3} \frac{\partial}{\partial x_i} \left( \frac{\partial \sigma_{kl}}{\partial x_k} \right) \right. \\
&\quad \left. - G_{ik} G_{kj} - G_{jk} G_{ki} + \frac{2\delta_{ij}}{3} G_{kl} G_{lk} \right), \tag{A 9}
\end{aligned}$$

using the substitution  $\rho(Du_i/Dt) = (\partial\sigma_{ij}/\partial x_j)$  (momentum conservation). Since terms proportional to  $T\epsilon^2$  are incorporated in the expression for  $T_{ij}^{(2)}$ , it is sufficient to incorporate the leading-order contribution to the stress in an expansion in  $\epsilon$ , which is given by  $(-p\delta_{ij})$  from (15) for the stress tensor.

$$\begin{aligned}
\frac{DS_{ij}}{Dt} &= -\frac{1}{2} \left( \frac{\partial}{\partial x_i} \left( \frac{1}{\rho} \frac{\partial p}{\partial x_j} \right) + \frac{\partial}{\partial x_j} \left( \frac{1}{\rho} \frac{\partial p}{\partial x_i} \right) - \frac{2\delta_{ij}}{3} \frac{\partial}{\partial x_k} \left( \frac{1}{\rho} \frac{\partial p}{\partial x_k} \right) \right. \\
&\quad \left. + G_{ik} G_{kj} + G_{jk} G_{ki} - \frac{2\delta_{ij}}{3} G_{kl} G_{lk} \right). \tag{A 10}
\end{aligned}$$

The term proportional to the substantial derivative of  $T$  is simplified using (16) for  $(DT/Dt)$ .

$$\frac{Q(\phi)S_{ij}}{2T^{1/2}} \frac{DT}{Dt} = -\frac{QS_{ij}}{2T^{1/2}} \frac{2T(1+4\phi\chi)G_{kk}}{3} \tag{A 11}$$

These are inserted into the second moment equation to obtain the second correction to the stress tensor,

$$\begin{aligned}
\epsilon^2 T_{ij}^{(2)} &= \frac{5}{16\sqrt{\pi}} \left( \frac{\pi Q}{6\phi\chi} - \frac{16\sqrt{\pi}Q^2}{35} + \frac{64\sqrt{\pi}}{105} - \frac{16\pi Q}{105} \right) (S_{ik}S_{kj} - (\delta_{ij}/3)S_{kl}S_{lk}) \\
&\quad - \frac{5\sqrt{\pi}Q}{96\phi\chi} (A_{ik}A_{kj} - (1/3)\delta_{ij}A_{kl}A_{lk} - A_{ik}S_{kj} - A_{jk}S_{ki}) \\
&\quad + \left( \frac{5\sqrt{\pi}Q}{144\phi\chi} \left( 1 - 2\phi\chi - \frac{3}{2Q} \frac{d(Q\rho)}{d\rho} \right) - \frac{\sqrt{\pi}Q}{9} + \frac{2}{9} \right) S_{ij}G_{kk} \\
&\quad - \frac{5\sqrt{\pi}Q}{192\phi\chi} \left( \frac{\partial}{\partial x_i} \left( \frac{1}{\rho} \frac{\partial p}{\partial x_j} \right) + \frac{\partial}{\partial x_j} \left( \frac{1}{\rho} \frac{\partial p}{\partial x_i} \right) - \frac{2\delta_{ij}}{3} \frac{\partial}{\partial x_k} \left( \frac{1}{\rho} \frac{\partial p}{\partial x_k} \right) \right), \tag{A 12}
\end{aligned}$$

where  $A_{ij} = (G_{ij} - G_{ji})/2$  is the antisymmetric part of the rate of deformation tensor.

This is inserted into the second moment equation, and the trace of the resulting equation is the energy balance equation,

$$\rho C_v \frac{DT}{Dt} + p(\phi, T)G_{ii} - 2\mu(\phi, T)S_{ik}S_{ki} - \mu_b(\phi, T)G_{ii}^2 + \epsilon^2 R(\phi)T^{3/2} = 0, \tag{A 13}$$

where  $p(\phi, T)$ ,  $\mu(\phi, T)$  and  $\mu_b(\phi, T)$  and  $R(\phi)$  are

$$p = \rho T(1 + (4 - 2\epsilon^2)\phi\chi(\phi)), \tag{A 14}$$

$$\mu(\phi) = \frac{5T^{1/2}}{16\sqrt{\pi}\chi(\phi)} \left( 1 + \frac{8\phi\chi(\phi)}{5} \right)^2 + \frac{48\phi^2\chi(\phi)T^{1/2}}{5\pi^{3/2}}, \tag{A 15}$$

$$\mu_b(\phi) = \frac{16\phi^2\chi T^{1/2}}{\pi^{3/2}}, \tag{A 16}$$

$$R(\phi) = 4\sqrt{\pi}\rho^2\chi(\phi), \tag{A 17}$$

and  $C_v = 3/2$  is the specific heat at constant volume. For a steady and spatially homogeneous flow with  $(DT/Dt) = 0$ , (A 13) is easily solved to determine  $T$

$$T^{1/2} = \left( \frac{-M(\phi)G_{ii} + (M(\phi)^2 G_{ii}^2 + 4\epsilon^2 N(\phi) S_{ij} S_{ji} + (4\epsilon^2 G_{ii}^2/9))^{1/2}}{2\epsilon^2} \right), \quad (\text{A } 18)$$

where the positive sign is assumed in the root of the quadratic equation because of the requirement that  $T^{1/2}$  has to be positive so that the viscosity is positive, and  $M(\phi)$  and  $N(\phi)$  are

$$\left. \begin{aligned} M(\phi) &= \sqrt{\pi} \left( \frac{1}{6} + \frac{1}{24\phi\chi(\phi)} \right), \\ N(\phi) &= \left( \frac{\sqrt{\pi}Q(\phi)}{24\phi\chi(\phi)} + \frac{2}{15} + \frac{\sqrt{\pi}Q(\phi)}{15} \right). \end{aligned} \right\} \quad (\text{A } 19)$$

Equation (A 18) reveals that the scaling of the mean square velocity of the particles is sensitive to the type of flow. For a radial flow with  $G_{ii} \neq 0$ , the leading-order temperature scales as  $T \sim (G_{ii}^2/\epsilon^4)$ , whereas for a flow with no radial component ( $G_{ii} = 0$ ), the temperature has the form  $T \sim (S_{ij}S_{ji}/\epsilon^2)$ , as indicated in (8). The scalings in (9) and (10) then follow from (A 4) and (A 12). For a spatially inhomogeneous flow with  $(DT/Dt) \neq 0$ , the leading-order approximation for (A 13) is

$$\begin{aligned} \frac{DT}{Dt} &= -\frac{2}{3}(1 + 4\phi\chi(\phi))TG_{ii} \\ &= -\frac{2pG_{ii}}{3\rho}. \end{aligned} \quad (\text{A } 20)$$

This is identical to the leading-order solution for the energy balance equation in an inviscid fluid, and has been used in A 11.

The constitutive relation for the stress tensor is now evaluated. The stress  $\sigma_{ij}$ , which is the rate of transport, per unit area, of  $i$ -momentum across a surface whose unit normal is in the  $j$ -direction, consists of two parts. The first is the kinetic part  $\sigma_{ij}^{(k)}$ , which is due to the physical transport of particles across the surface, and the other is the collisional part  $\sigma_{ij}^{(c)}$ , which is due to the collision of particles on one side of the surface with particles on the other side,

$$\begin{aligned} \sigma_{ij}^{(k)} &= -\rho \langle c_i c_j \rangle \\ &= -\rho (T\delta_{ij} + \epsilon^{1/2} T_{ij}^{(1)} + \epsilon T_{ij}^{(2)}), \end{aligned} \quad (\text{A } 21)$$

$$\begin{aligned} \sigma_{ij}^{(c)} &= \frac{1}{2}\rho^2 d^3 \chi(\phi) \int_{\mathbf{k}} \int_{\mathbf{u}} \int_{\mathbf{u}^*} f(\mathbf{x}, \mathbf{u}) f(\mathbf{x}^*, \mathbf{u}^*) (c'_i - c_i) k_j (\mathbf{u} - \mathbf{u}^*) \cdot \mathbf{k} \\ &= \frac{6\rho\phi\chi(\phi)}{\pi} \left( \frac{-2\pi T}{3} + \frac{8\sqrt{\pi T} S_{ij}}{15} + \frac{4\sqrt{\pi T} \delta_{ij} G_{kk}}{9} \right. \\ &\quad - \frac{4\pi}{15} (\epsilon T_{ij}^{(1)} + \epsilon^2 T_{ij}^{(2)}) + \frac{\pi\epsilon^2 \delta_{ij}}{6} (2 + T^{-1} T_{kl}^{(1)} T_{lk}^{(1)}) \\ &\quad - \frac{2\pi}{105} (4S_{ik} S_{kj} + \delta_{ij} S_{kl} S_{lk}) - \frac{4\pi S_{ij} G_{kk}}{45} - \frac{\pi \delta_{ij} G_{kk}^2}{27} \\ &\quad \left. + \frac{4\sqrt{\pi}\epsilon T^{-1/2}}{105} \left( \frac{7}{3} T_{ij}^{(1)} G_{kk} + 2(T_{ik}^{(1)} S_{kj} + T_{jk}^{(1)} S_{ki}) + \delta_{ij} T_{kl}^{(1)} S_{lk} \right) \right). \end{aligned} \quad (\text{A } 22)$$



Adding the two contributions, we obtain the familiar form of the stress tensor given in (15), where  $p$ ,  $\mu$  and  $\mu_b$  are given in (A 14)–(A 16) and the coefficients  $\mathcal{A}$  to  $\mathcal{G}$  are

$$\rho^{-1}\mathcal{A}(\phi) = -\left(\frac{5}{16\sqrt{\pi}} + \frac{\phi\chi(\phi)}{2\sqrt{\pi}}\right) \left(\frac{Q\pi}{6\phi\chi(\phi)} - \frac{16\sqrt{\pi}Q^2}{35} + \frac{64\sqrt{\pi}}{105} - \frac{16\pi Q}{105}\right) - \frac{16\phi\chi(\phi)}{35} - \frac{32Q\phi\chi(\phi)}{35\sqrt{\pi}}, \quad (\text{A } 23)$$

$$\rho^{-1}\mathcal{B}(\phi) = \left(\frac{5}{48\sqrt{\pi}} + \frac{\phi\chi(\phi)}{6\sqrt{\pi}}\right) \left(\frac{Q\pi}{6\phi\chi(\phi)} - \frac{16\sqrt{\pi}Q^2}{35} + \frac{64\sqrt{\pi}}{105} - \frac{16\pi Q}{105}\right) + \phi\chi(\phi)Q^2 - \frac{4\phi\chi(\phi)}{35} - \frac{8\phi\chi(\phi)Q}{35\sqrt{\pi}}, \quad (\text{A } 24)$$

$$\rho^{-1}\mathcal{C}(\phi) = -\frac{2\pi\phi\chi(\phi)}{9}, \quad (\text{A } 25)$$

$$\rho^{-1}\mathcal{D}(\phi) = -\left(1 + \frac{8\phi\chi(\phi)}{5}\right) \left(\frac{5\sqrt{\pi}Q}{144\phi\chi} \left(1 - 2\phi\chi - \frac{3}{2Q} \frac{d(Q\rho)}{d\rho}\right) + \frac{\sqrt{\pi}Q}{9} - \frac{2}{9}\right) - \frac{8\phi\chi}{15} - \frac{8Q\phi\chi}{15\sqrt{\pi}}, \quad (\text{A } 26)$$

$$\rho^{-1}\mathcal{E}(\phi) = -\frac{5\sqrt{\pi}Q}{96\phi\chi} \left(1 + \frac{8\phi\chi}{5}\right), \quad (\text{A } 27)$$

$$\rho^{-1}\mathcal{F}(\phi) = \frac{5\sqrt{\pi}Q}{96\phi\chi} \left(1 + \frac{8\phi\chi}{5}\right), \quad (\text{A } 28)$$

$$\rho^{-1}\mathcal{G}(\phi) = \frac{5\sqrt{\pi}Q}{192\phi\chi} \left(1 + \frac{8\phi\chi}{5}\right). \quad (\text{A } 29)$$

## Appendix B

The elements of the matrix  $\mathbf{A}$  in (45) in the Burnett approximation are,

$$\begin{aligned} \Lambda_{\rho\rho} &= 0, & \Lambda_{\rho x} &= ik\bar{\rho}, & \Lambda_{\rho y} &= il\bar{\rho}, & \Lambda_{\rho z} &= im\bar{\rho}, & \Lambda_{\rho T} &= 0, \\ \bar{\rho}\Lambda_{x\rho} &= i(-\bar{G}l\bar{\mu}_\rho + k(\bar{p}_\rho + \bar{G}^2(-\bar{\mathcal{A}}_\rho/4 - \bar{\mathcal{C}}_\rho/2 - \bar{\mathcal{E}}_\rho/2 + \bar{\mathcal{F}}_\rho/12))) \\ &\quad - \frac{2ik\bar{p}_\rho\bar{\mathcal{G}}}{3\bar{\rho}}(2k^2 - kl + 3l^2 + 2m^2), \\ \bar{\rho}\Lambda_{xx} &= \bar{\rho}s + \bar{\mu}(4k^2/3 + 2l^2 + m^2) + \bar{\mu}_bk^2 + kl\bar{G}(2\bar{\mathcal{A}}/3 + \bar{\mathcal{C}} + \bar{\mathcal{D}}/2 + \bar{\mathcal{E}}/2 - \bar{\mathcal{F}}/6), \\ \bar{\rho}\Lambda_{xy} &= \bar{\rho}\bar{G} + (4kl\bar{\mu}/3) + kl\bar{\mu}_b + \bar{\mathcal{A}}\bar{G}((k^2/2) + (l^2/6) + (m^2/4)) + \bar{\mathcal{C}}\bar{G}k^2 + (\bar{\mathcal{D}}\bar{G}l^2/2) \\ &\quad + \bar{\mathcal{E}}\bar{G}l^2/2 + \bar{\mathcal{F}}\bar{G}(k^2/6 + k^2/4), \\ \bar{\rho}\Lambda_{xz} &= (\bar{\mu}km/3) + \bar{\mu}_bkm + \bar{G}lm(-\bar{\mathcal{A}}/12 + \bar{\mathcal{D}}/2 + \bar{\mathcal{E}}/2 - \bar{\mathcal{F}}/4), \\ \bar{\rho}\Lambda_{xT} &= -\frac{2ik\bar{p}_\rho\bar{\mathcal{G}}}{3\bar{\rho}}(2k^2 - kl + 3l^2 + 2m^2) + \frac{i(k\bar{p} - l\bar{\mu}/2)}{\bar{T}}, \\ \bar{\rho}\Lambda_{y\rho} &= i(l\bar{p}_\rho - \bar{G}k\bar{\mu}_\rho - l\bar{G}^2(\bar{\mathcal{A}}_\rho/4 + \bar{\mathcal{C}}_\rho/2 - \bar{\mathcal{E}}_\rho/2 - \bar{\mathcal{F}}_\rho/12)) \\ &\quad + \frac{2il\bar{p}_\rho\bar{\mathcal{G}}}{3\bar{\rho}}(k^2 - 5kl - 2m^2), \end{aligned}$$

$$\begin{aligned}
\bar{\rho}\Lambda_{yx} &= (\bar{\mu}kl/3) + kl\bar{\mu}_b + \bar{G}\bar{\mathcal{A}}(k^2/6 + l^2/2 + m^2/4) + \bar{\mathcal{C}}\bar{G}l^2 + (\bar{\mathcal{D}}\bar{G}k^2/2) \\
&\quad - \bar{\mathcal{E}}\bar{G}(k^2/2 + l^2 + m^2) - \bar{\mathcal{F}}\bar{G}(l^2/6 + m^2/4), \\
\bar{\rho}\Lambda_{yy} &= s\bar{\rho} + \bar{\mu}(4l^2/3 + k^2 + m^2) + \bar{\mu}_b l^2 \\
&\quad + \bar{G}kl(2\bar{\mathcal{A}}/3 + \bar{\mathcal{C}} + \bar{\mathcal{D}}/2 + \bar{\mathcal{E}}/2 + \bar{\mathcal{F}}/6), \\
\bar{\rho}\Lambda_{yz} &= (\bar{\mu}lm/3) + lm\bar{\mu}_b + \bar{G}km(-\bar{\mathcal{A}}/12 + \bar{\mathcal{D}}/2 + \bar{\mathcal{E}}/2 - \bar{\mathcal{F}}/4), \\
\bar{\rho}\Lambda_{yT} &= \frac{2i\bar{l}\bar{p}\bar{\mathcal{G}}}{3\bar{\rho}}(k^2 - 5kl - 2m^2) + \frac{i(l\bar{p} - k\bar{\mu}/2)}{\bar{T}}, \\
\bar{\rho}\Lambda_{z\rho} &= im\bar{p}_\rho - i\bar{G}^2m(\bar{\mathcal{C}}_\rho/2 + \bar{\mathcal{F}}_\rho/6) - \frac{2im\bar{p}_\rho\bar{\mathcal{G}}}{3\bar{\rho}}(2k^2 - kl + 3l^2 + 2m^2), \\
\bar{\rho}\Lambda_{zx} &= km(\bar{\mu}_b + \bar{\mu}/3) + \bar{G}lm(\bar{\mathcal{A}}/4 + \bar{\mathcal{C}} - \bar{\mathcal{E}}/2 + \bar{\mathcal{F}}/12), \\
\bar{\rho}\Lambda_{zy} &= lm(\bar{\mu}_b + \bar{\mu}/3) + km\bar{G}(\bar{\mathcal{A}}/4 + \bar{\mathcal{C}} - \bar{\mathcal{F}}/12), \\
\bar{\rho}\Lambda_{zz} &= s\bar{\rho} + \bar{\mu}(4m^2/3 + k^2 + l^2) + m^2\bar{\mu}_b + kl\bar{G}(\bar{\mathcal{A}}/2 + \bar{\mathcal{E}}/2), \\
\bar{\rho}\Lambda_{zT} &= \frac{-2i\bar{p}m}{3\bar{\rho}}(2k^2 - kl + 3l^2 + m^2) + \frac{im\bar{p}}{\bar{T}}, \\
\bar{\rho}C_v\Lambda_{T\rho} &= \epsilon^2\bar{R}_\rho\bar{T}^{3/2} - \bar{G}^2\bar{\mu}_\rho, \\
\bar{\rho}C_v\Lambda_{Tx} &= ik\bar{p} - 2i\bar{G}l\bar{\mu}, \\
\bar{\rho}C_v\Lambda_{Ty} &= il\bar{p} - 2i\bar{G}k\bar{\mu}, \\
\bar{\rho}C_t\Lambda_{Tz} &= im\bar{p}, \\
\bar{\rho}C_t\Lambda_{TT} &= \frac{3\bar{R}\epsilon^2\bar{T}^{1/2}}{2} - \frac{\bar{G}^2\bar{\mu}}{2\bar{T}}.
\end{aligned}$$

Here, the first subscript for  $\Lambda$  refers to the conservation equation ( $\rho$  for the density conservation,  $x$ ,  $y$  and  $z$  for the momentum conservation in the respective directions and  $T$  for the energy conservation equation), and the second refers to the perturbation variable (density, velocity in the three directions and temperature) multiplied by this coefficient.

## REFERENCES

- ALLEN, M. P. & TILDESLEY, D. J. 1990 *Computer Simulations of Liquids*. Clarendon.
- BABIC, C. 1993 On the stability of rapid granular flows. *J. Fluid Mech.* **254**, 127–150.
- CHAPMAN, S. & COWLING, T. G. 1970 *The Mathematical Theory of Non-uniform Gases*. Cambridge University Press.
- ERNST, M. H., CICHOCKI, B., DORFMAN, J. R., SHARMA, J. & VAN BEIJEREN, H. 1978 Kinetic theory of nonlinear viscous flow in two and three dimensions. *J. Stat. Phys.* **18**, 237–270.
- HANSEN, J. P. & MCDONALD, I. 1990 *Theory of Simple Liquids*. Academic.
- JENKINS, J. T. & RICHMAN, M. W. 1985 Grad's 13-moment system for a dense gas of inelastic spheres. *Arch. Rat. Mech. Anal.* **87**, 355–377.
- JENKINS, J. T. & RICHMAN, M. W. 1986 Boundary conditions for plane flows of smooth, nearly elastic, circular disks. *J. Fluid Mech.* **171**, 53–69.
- JENKINS, J. T. & RICHMAN, M. W. 1988 Plane simple shear of smooth inelastic circular disks: the anisotropy of the second moment in the dilute and dense limits. *J. Fluid Mech.* **192**, 313–328.
- JENKINS, J. T. & SAVAGE, S. B. 1983 A theory for the rapid flow of identical, smooth, nearly elastic particles. *J. Fluid Mech.* **130**, 186–202.
- JIN, S. & SLEMROD, M. 2001 Regularisation of the Burnett equations for rapid granular flows via relaxation. *Physica D* **150**, 207–218.

- KAMGAR-PARSI, B. & COHEN, E. G. D. 1986 Eigenmodes of a dilute simple gas in equilibrium. *Physica A* **138**, 249–268.
- KUMARAN, V. 2001a, Anomalous behaviour of hydrodynamic modes in the two dimensional shear flow of a granular material. *Physica A*, **293**, 385.
- KUMARAN, V. 2001b, Hydrodynamic modes of a sheared granular flow from the Boltzmann and Navier–Stokes equations. *Phys. Fluids* **13**, 2258.
- LUN, C. K. K., SAVAGE, S. B., JEFFREY, D. J. & CHEPURNIY, N. 1984 Kinetic theories for granular flow: inelastic particles in Couette flow and slightly inelastic particles in a general flow field. *J. Fluid Mech.* **140**, 223–256.
- RESIBOIS P. & DE LEENER, M. 1977 *Classical Kinetic Theory of Fluids*. Wiley.
- SAVAGE, S. B. 1992 Instability of unbounded uniform granular flow. *J. Fluid Mech.* **241**, 109–123.
- SAVAGE, S. B. & JEFFREY, D. J. 1981 The stress tensor in a granular flow at high shear rates. *J. Fluid Mech.* **110**, 255–272.
- SCHMID, P. J. & KYTOMAA, H. K. 1994 Transient and asymptotic stability of granular shear flow. *J. Fluid Mech.* **264**, 255–275.
- SELA, N. & GOLDBIRSCHE, I. 1998 Hydrodynamic equations for rapid flows of smooth inelastic spheres, to Burnett order. *J. Fluid Mech.* **361**, 41–74.
- SELA, N., GOLDBIRSCHE, I. & NOSKOWICZ, S. H. 1996 Kinetic theoretical study of a simply sheared two dimensional granular gas to Burnett order, *Phys. Fluids* **8**, 2337.
- WANG, C.- H., JACKSON, R. & SUNDARESAN, S. 1996 Stability of bounded rapid shear flows of a granular material. *J. Fluid Mech.* **308**, 31–62.